Article

Current Biology

Sleep neuron depolarization promotes protective gene expression changes and FOXO activation

Graphical abstract

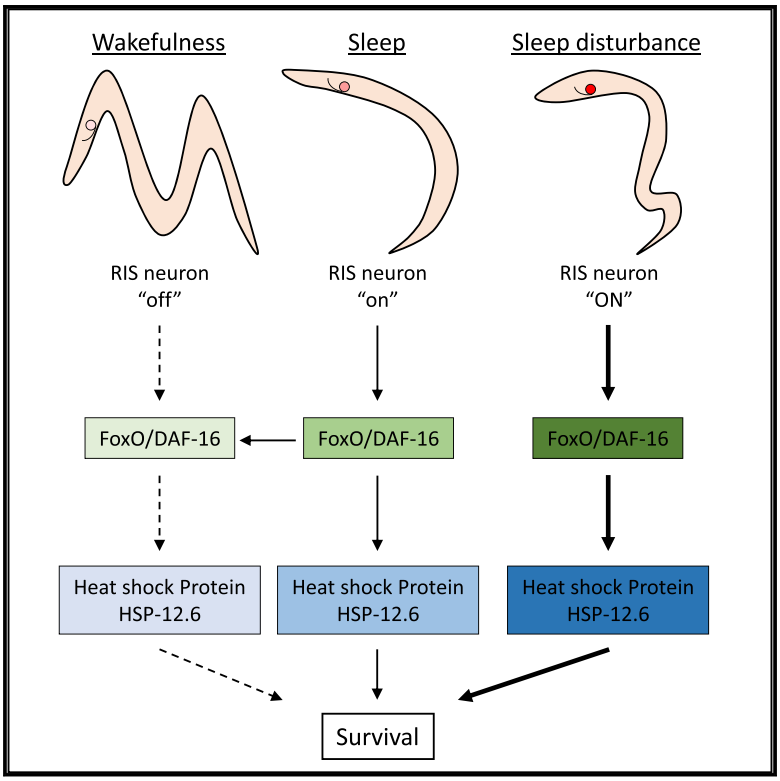

Highlights

- The sleep neuron RIS promotes protective gene expression changes during larval arrest
- RIS depolarization promotes FOXO/DAF-16 activation and chaperone expression
- RIS depolarization promotes survival through FOXO/DAF-16 and chaperone expression
- Disturbed sleep overactivates RIS to boost gene expression changes and survival

Authors

Anastasios Koutsoumparis, Luisa M. Welp, Alexander Wulf, ..., Bernd Timmermann, Inka Busack, Henrik Bringmann

Correspondence

henrik.bringmann@tu-dresden.de

In brief

Koutsoumparis et al. show that the sleep-active RIS neuron in *C. elegans* depolarizes during sleep to promote protective gene expression changes, including the activation of FOXO and chaperone expression, thus promoting survival. Disturbing sleep further increases RIS activity and thus further promotes gene expression and survival.

Koutsoumparis et al., 2022, Current Biology *32*, 2248–2262
May 23, 2022
https://doi.org/10.1016/j.cub.2022.04.012

CellPress

CellPress

Current Biology

Article

Sleep neuron depolarization promotes protective gene expression changes and FOXO activation

Anastasios Koutsoumparis,[1] Luisa M. Welp,[2] Alexander Wulf,[2] Henning Urlaub,[2,3] David Meierhofer,[4] Stefan Börno,[5] Bernd Timmermann,[5] Inka Busack,[1] and Henrik Bringmann[1,6,7,*]

[1]Chair of Cellular Circuits and Systems, Biotechnology Center (BIOTEC), Center for Molecular and Cellular Bioengineering (CMCB), Technical University Dresden, 01307 Dresden, Germany

[2]Bioanalytical Mass Spectrometry Group, Max Planck Institute for Multidisciplinary Sciences, 37077 Göttingen, Germany

[3]Bioanalytics Group, Institute for Clinical Chemistry, University Medical Center Göttingen, 37075 Göttingen, Germany

[4]Mass Spectrometry Facility, Max Planck Institute for Molecular Genetics, 14195 Berlin, Germany

[5]Sequencing Core Facility, Max Planck Institute for Molecular Genetics, 14195 Berlin, Germany

[6]Twitter: @BIOTEC_TUD

[7]Lead contact

*Correspondence: henrik.bringmann@tu-dresden.de

https://doi.org/10.1016/j.cub.2022.04.012

SUMMARY

Sleep is an essential state that allows for recuperation and survival processes. Disturbing sleep triggers stress responses that promote protective gene expression. Sleep and its deprivation grossly impact gene expression, but little is known about how normal or disturbed sleep control gene expression. Central to the induction of sleep are sleep-active neurons, which inhibit wakefulness and promote survival. Sleep and sleep-active neurons are highly conserved. In *Caenorhabditis elegans*, the sleep-active RIS neuron is crucial for sleep and survival. Here, we show that RIS depolarization promotes the protective gene expression response that occurs during developmental arrest. This response includes the activation of FOXO/DAF-16 and expression of DAF-16 target genes such as HSP-12.6, a small heat-shock protein that is required for starvation survival. Disturbing sleep by mechanical stimulation increases RIS depolarization. RIS activation in turn activates DAF-16 and other genes required for survival. Hence, during normal sleep, RIS depolarization promotes protective gene expression. When sleep is disturbed, protective gene expression gets further increased by raised RIS depolarization. We thus link sleep-active neuron depolarization to protective gene expression changes and suggest that the cellular stress response following sleep deprivation could be understood as a safeguarding process that is caused by the overactivation of sleep-active neurons.

INTRODUCTION

Sleep and wakefulness are characterized by large oscillations in gene expression that affect cellular physiology broadly to support core functions of sleep for building, repair, and plasticity.[1,2] Sleep deprivation triggers systemic and cellular stress responses.[3–5] Cellular stress responses include the increased expression of protective genes encoding cytosolic chaperones, components of the unfolded protein response (UPR) in ER and mitochondria, as well as oxidative stress and DNA damage pathway genes.[5] Sleep deprivation induces large transcriptional responses[1,2] and activation of transcription factors such as FOXO.[6,7] Cellular stress responses, in turn, can mitigate the lethal effects that are often caused by sleep deprivation.[6,8] On the other hand, overactive stress responses following sleep deprivation can have detrimental consequences for health, in particular when they are activated for extended periods of time.[3,5]

Across species, sleep-active neurons depolarize to inhibit wakefulness circuits through GABA and neuropeptides and thus cause sleep.[9,10] Sensory stimulation can at first suppress the activity of sleep-active neurons and force wakefulness, but sensory stimulation also typically causes an overactivation of sleep-active neurons, eventually causing a return to sleep or compensatory increases in sleep depth or sleep time, thus forming homeostatic mechanisms.[11,12]

Sleep deprivation is a key approach to study sleep functions. The sleep deprivation procedure, which typically includes strong sensory stimulation to cause hyperarousal and thus wakefulness, can however be stressful and thus can trigger stress responses.[13,14] This means that the stress responses observed after sleep deprivation may not be caused only by the loss of sleep but also by the stressor. Another possible explanation for the increased stress response following sleep disturbance could be that the absence of sleep per se prevents an essential function of sleep from being fulfilled, thus causing cellular stress, which in turn triggers cellular stress responses. Similarly, increased wakefulness could promote stress.[5,15] An alternative, yet less explored, possibility is that sleep deprivation enhances the normal functions of sleep, which could be the promotion of

cell-protective processes that are similar to cellular stress responses. Disturbed sleep triggers homeostatic compensation mechanisms that include the overactivation of sleep-active neurons, which can lead to a subsequent increase in sleep depth or time asleep.[16,17] If the sleep circuits promote cell-protective processes during normal sleep, an increased activity of the sleep circuits could thus trigger an increased activity of cell-protective processes. As it is unclear what causes the consequences of sleep deprivation, it is difficult to deduce sleep functions from sleep deprivation experiments.[16] A key challenge in sleep research thus is to solve the mechanisms by which sleep affects protective functions and to understand how sleep deprivation affects stress responses and protective gene expression.

Sleep in *C. elegans* requires the GABAergic and peptidergic sleep-active RIS neuron.[18] RIS depolarizes specifically during sleep to inhibit wakefulness circuits through FLP-11 neuropeptides and perhaps also GABA, and RIS impairment virtually abolishes sleep during many stages and conditions.[18–21] Various stressors promote protective sleep.[22–26] For example, starvation during the first larval stage (L1) causes a developmental arrest that involves a transcriptional response that halts growth and shifts the physiology toward stress resistance and energy conservation.[27,28] RIS depolarizes during L1 arrest to increase sleep and promote survival.[29] However, how RIS supports survival is not understood.

Here, we tested the role of RIS in the protective gene expression response that occurs during L1 arrest. We show that the activity of the RIS neuron promotes the protective gene expression response, including FOXO activation and chaperone expression. Disturbing sleep by mechanical stimulation increases the activation of the RIS neuron, which in turn boosts protective gene expression. Thus, sleep-active neuron depolarization promotes protective gene expression during normal sleep, and disturbance during sleep over activates the sleep neuron to further increase protective gene expression.

RESULTS

APTF-1 promotes the protective gene expression response that occurs during larval starvation

Larval starvation triggers the arrest of development and a massive transcriptional response affecting hundreds of genes.[27,28] Here, we tested the role of RIS in the protective gene expression response during L1 arrest using a multi-omics approach. We first performed a transcriptome analysis of L1 arrest in worms in which RIS was dysfunctional. For this experiment, RIS was impaired by deletion of the AP2 transcription factor gene *aptf-1 (aptf-1(gk794))* that is required for the expression of sleep-promoting neuropeptides in RIS.[18,19] We determined the transcriptomes of wild-type and *aptf-1(gk794)* L1 larvae both during development (in the presence of food) as well as during developmental arrest (after 48 h of starvation) and first determined genes that were differentially expressed during the arrest ($|\text{Log}_2\ \text{FC}| > 1$ and FDR < 5%). The transcriptome analysis showed that in the wild type during L1 arrest, 1,480 genes were down-regulated and 1,653 genes were upregulated (Figure 1A; Data S1). During L1 arrest in *aptf-1(gk794)*, only 816 genes were down-regulated and only 865 genes were up-regulated (Figure 1B; Data S1). Thus, the gene expression response during arrest in *aptf-1(gk794)* animals appeared to be much less pronounced compared with wild type.

We next used the genes that were differentially expressed during the arrest compared with development in the transcriptomes of wild-type worms to define the L1-arrest gene expression response. We then tested whether the expression of these arrest-regulated genes was affected in *aptf-1(gk794)*. Many of the genes that were up-regulated during arrest in the wild type were also up-regulated in *aptf-1(gk794)*, but the response was dampened and the level of up-regulation was reduced. Similarly, many of the genes that were down-regulated during the arrest in the wild type, were down-regulated also in *aptf-1(gk794)*, but the down-regulation was again dampened (Figure 1E).

We next used isobaric chemical labeling and mass spectrometry to perform a relative quantification of the proteomes of larvae that were grown under the same conditions as for the transcriptome analysis. The proteome analysis confirmed the dampened expression of arrest-specific genes, with 440 proteins showing altered expression ($|\text{Log}_2\ \text{FC}| > 1$) in the wild type and only 307 proteins showing altered expression in *aptf-1(-)* (Figures 1C and 1D; Data S2). Again, many proteins that were up-regulated during arrest in the wild type were expressed at lower levels in *aptf-1(gk794)*, and proteins that were down-regulated during arrest in the wild type were expressed at higher levels in *aptf-1(gk794)* (Figure 1F). Thus, *aptf-1(gk794)* blunts the gene expression changes during the arrest.

APTF-1 broadly supports protective gene expression and promotes DAF-16 target gene expression

Gene Ontology (GO) term analysis of RNA sequencing (RNA-seq) data in L1 arrest indicated that *aptf-1(gk794)* reduced the expression of components of the gene expression machinery, including factors required for chromatin organization, splicing, and translation. Also, genes required for mitochondrial gene expression and function showed reduced expression. By contrast, genes associated with neuropeptidergic transmission showed increased expression (Figure 2A; Data S3). The broad effect on general components of the gene expression system as well as the alterations of neuronal transmission suggested that genes required for gene expression are broadly affected by neuronal signaling across multiple cell types. Gene set enrichment analysis indicated that multiple major tissues (intestine, hypodermis, muscle, neurons, and the germ line) were affected in *aptf-1(gk794)*, with intestine and germ line dominated by the down-regulation of genes, and the hypodermis and neurons dominated by up-regulation of genes (Figure 2B).

During the starvation response, FOXO remodels transcription to arrest development and rewire metabolism.[28,30] DAF-16 binds to and activates expression of genes whose promoter region contains the DAF-16 binding element (DBE).[31] Conversely, genes containing the DAF-16 associated element (DAE) are typically negatively controlled by DAF-16 and are bound by the PQM-1 transcriptional regulator.[32] We hence tested whether the differentially expressed genes in *aptf-1(gk794)* were enriched for DBE and DAE motifs or binding by DAF-16 or PQM-1. *aptf-1(gk794)* showed significantly reduced expression of genes that contain the DBE or that are bound by DAF-16, according to ChIP-seq data, whereas genes that contain the DAE or that are bound by PQM-1 showed a significant increase in expression

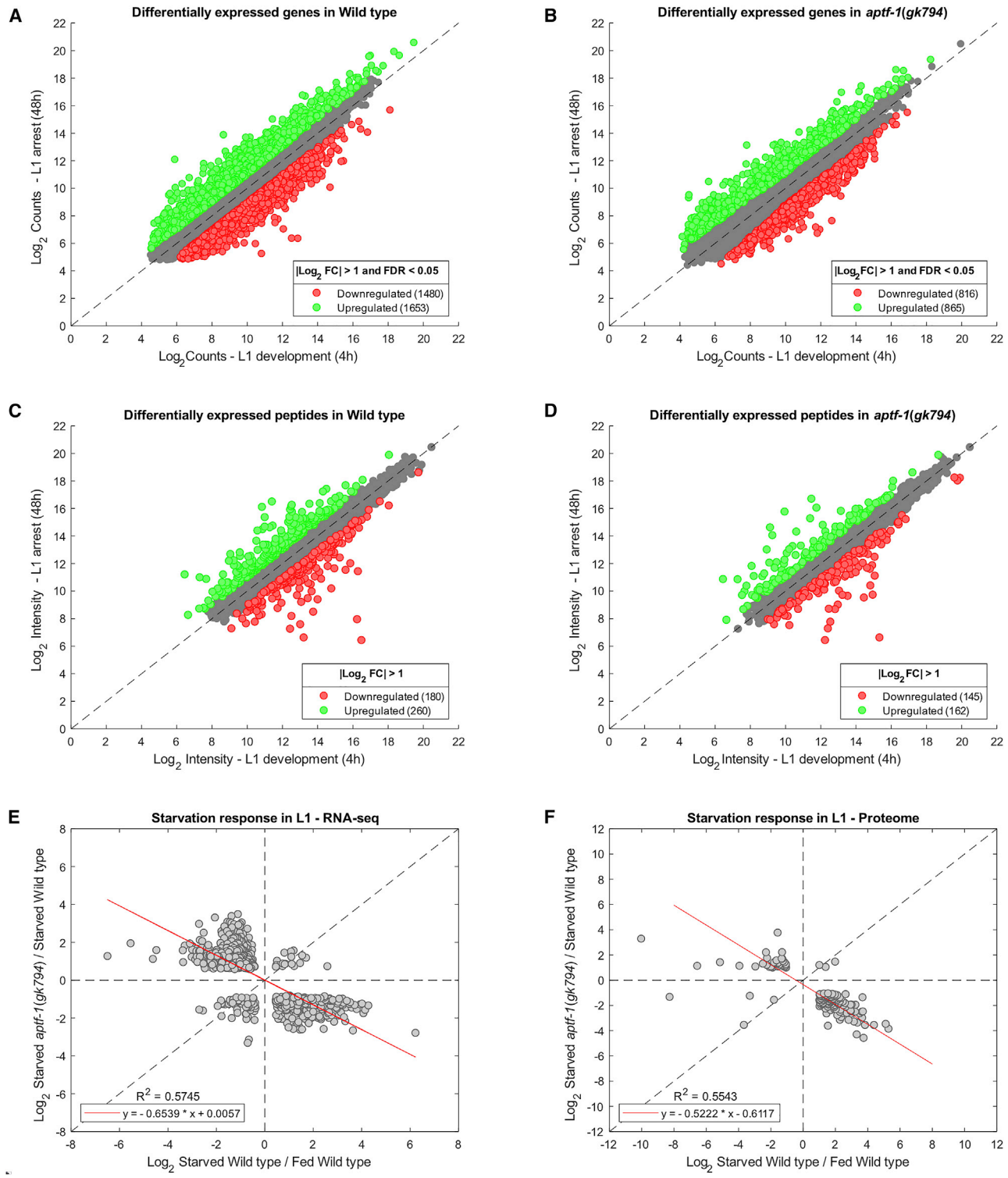

Figure 1. APTF-1 promotes the gene expression response during developmental arrest

(A and B) Scatterplot overview of RNA-seq data in (A) wild-type and (B) *aptf-1(gk794)* worms shows quantitative differences in gene expression during the starvation response. Statistically not significant entries according to the selected thresholds are marked in gray.

(C and D) Scatterplot overview of proteome data in (C) wild-type and (D) *aptf-1(gk794)* worms shows quantitative differences in protein expression during the starvation response. Entries with $|\text{Log}_2\ \text{FC}| < 1$ are marked in gray.

(E and F) *aptf-1(gk794)* caused a dampened starvation response on (E) the transcriptome and (F) the proteome levels.

Related data can be found in Data S1 and S2.

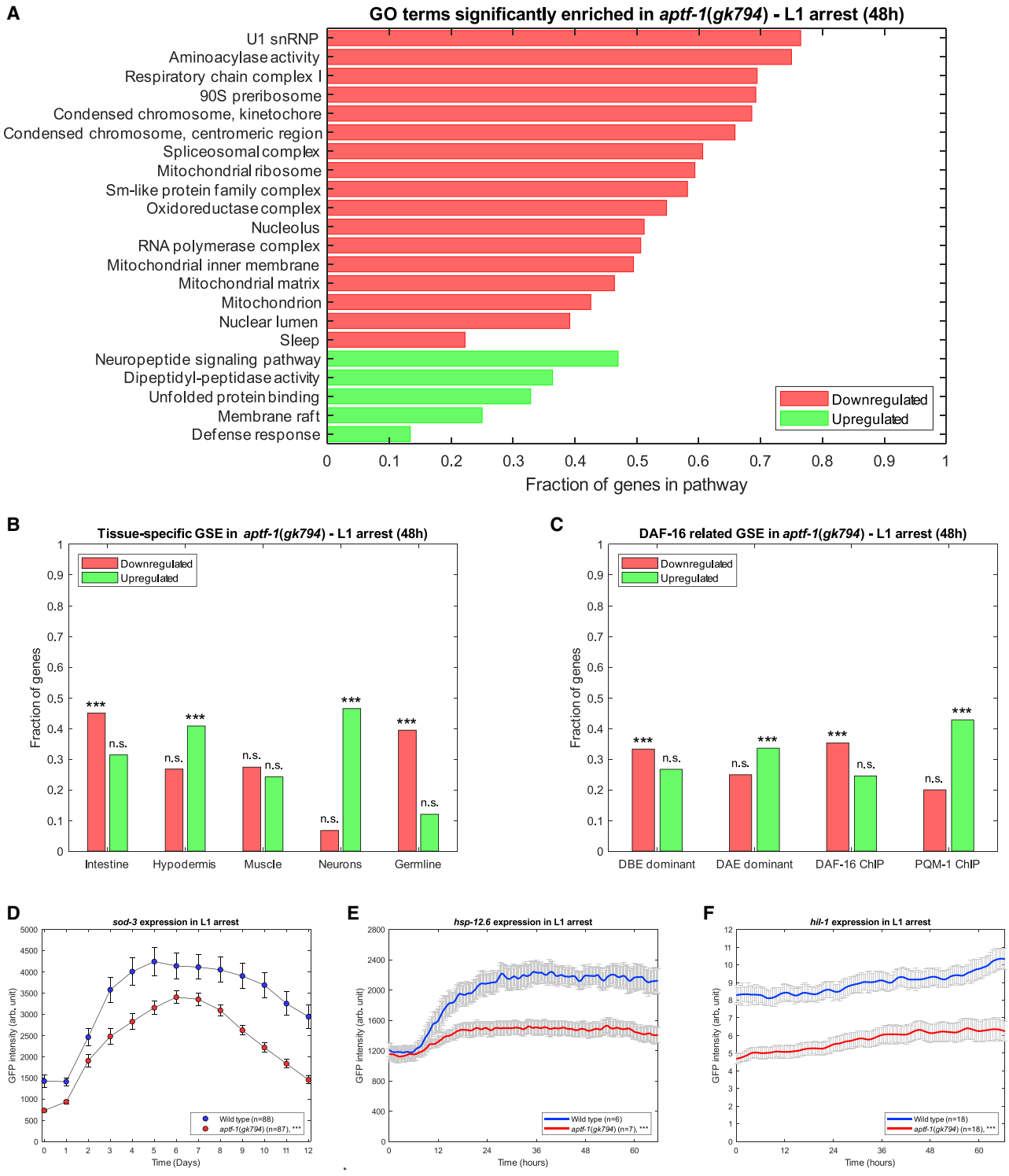

Figure 2. APTF-1 broadly supports gene expression including the expression of DAF-16 target genes

(A) GO term enrichment analysis of genes differentially expressed in *aptf-1(gk794)* during starvation reveals changes associated with gene expression and metabolic pathways. All of the pathways shown are significantly enriched with $p_{adj} < 0.05$. The full list of enriched GO terms can be found in Data S4.

(B) Gene set enrichment analysis for tissue-specific genes, shows significant down-regulation of intestine and germline genes, whereas hypodermis and neuron genes are significantly up-regulated. Statistical significance was assessed by Fisher's exact test with Bonferroni correction for multiple comparisons ***$p_{adj} < 0.001$, n.s., not significant.

(legend continued on next page)

(Figure 2C).To verify the effects of *aptf-1* on protective gene expression and to study the dynamics of the starvation-induced arrest gene expression response, we tested fluorescent transcriptional reporters for three genes that 1) carry the DBE sequence, 2) are expressed at lower levels in starved *aptf-1(gk794),* and 3) show DAF-16-dependent up-regulation during arrest. The three genes chosen were the small heat-shock protein gene *hsp-12.6*, the histone H1-like gene *hil-1*, and the superoxide dismutase gene *sod-3*.[31,33–36] Consistent with our transcriptome data, the expression of all of the three DBE-containing reporter genes was attenuated in *aptf-1(gk794)* (Figures 2D–2F). A label-free quantification mass spectrometric analysis of the proteome revealed that the correlation of transcriptome and proteome was moderate, which is consistent with previous analyses of adult starvation.[37] The mass spectrometry analysis validated the dampened expression of HSP-12.6 in *aptf-1(gk794)*, which motivated us to use this gene as a readout for subsequent analyses (Figure S1A; Data S4). To test whether *aptf-1(gk794)* was generally impaired in HSP-12.6 expression, we tested the expression of HSP-12.6 in response to a heat shock, which triggers high levels of expression of this molecular chaperone.[38] Following a heat shock, expression of HSP-12.6 in wild-type and *aptf-1(gk794)* larvae reached the same levels, indicating that *aptf-1(gk794)* is generally able to strongly express HSP-12.6 (Figure S1B). Thus, *aptf-1(gk794)* broadly blunts protective gene expression during L1 arrest, including the expression of genes that are controlled by DBE/DAF-16.

RIS depolarization controls DAF-16 target gene expression

aptf-1 is expressed in RIB, AIB, and RIS neurons, which we confirmed also during L1 arrest (Figure S2). It functions in sleep in the RIS neuron that depolarizes during many types of sleep to cause behavioral quiescence.[18,21,25,29,39,40] The majority of the effects of *aptf-1(gk794)* on gene expression were thus most likely caused by impaired RIS. It is possible though, that some of the changes observed in the omics analyses were caused by AIB or RIB. We did not investigate the roles of AIB and RIB further but focused on the contributions of RIS. A stable rescue of *aptf-1* in RIS has not yet been established, as RIS-specific genes typically are under the control of *aptf-1(-)*.[18–20] To clearly link RIS to gene expression during starvation, we hence tested how increased and decreased RIS activity affects gene expression. Phenotypes observed in both *aptf-1(-)* and after RIS inactivation can thus be assigned to RIS function with high confidence.

To test how RIS activity levels modulate gene expression and DAF-16 targets during L1 arrest, we studied strains in which RIS was either constantly hyperpolarized or depolarized through the expression of constitutively active ion channels.[41] For specific expression in RIS, we used the *flp-11* promoter that is highly enriched in RIS[39] and presents the most specific promoter available for RIS, according to single-cell sequencing data of the entire nervous system.[42] To hyperpolarize RIS, we used expression of a constitutively active potassium channel mutant in this neuron (*RIS::twk-18gf*); to depolarize RIS, we used a constitutively active K2P channel mutant that is permeable for sodium (*RIS::unc-58gf(strong)*).[43] By using these strains, it has been shown that hyperpolarization and surprisingly also constant strong depolarization of RIS both abolish sleep behavior. Sleep loss caused by constant depolarization may be caused by excessive transmission from RIS, which then causes desensitization of downstream neuronal circuits that generate wakefulness behavior.[41] Hence, these RIS-manipulating strains provide a chance to test whether the observed changes in gene expression are functions of sleep or RIS depolarization.

RNA-seq of *RIS::twk-18gf* and *RIS::unc-58gf(strong)* identified 141 differentially expressed genes in *RIS::twk-18gf* (66 down and 75 up) and 596 differentially expressed genes in RIS::*unc-58gf(strong)* (306 down and 290 up), (Figures 3A and 3B; Data S5, $|\text{Log}_2\ \text{FC}| > 1$ and FDR < 5%). There was a substantial negative correlation of the hyperpolarization and depolarization datasets; i.e., many of the genes that were up-regulated in *RIS::twk-18gf* were down-regulated in *RIS::unc-58gf(strong)*, and many of the genes that were down-regulated in *RIS::twk-18gf* were up-regulated in *RIS::unc-58gf(strong)* (87% of the significantly regulated genes in both conditions followed this anti-correlation pattern). For example, DBE-containing genes that are up-regulated during L1 arrest such as *hsp-12.6* and *sod-5* were down-regulated with RIS hyperpolarization and up-regulated with RIS depolarization (Figure 3C). A few DBE-containing genes including *icl-1* were up-regulated in *RIS::twk-18gf* and were down-regulated in *RIS::unc-58gf(strong)*. *icl-1* is required for the glyoxylate shunt during starvation, and its up-regulation during larval starvation depends only in part on *daf-16* but also on other factors,[33] which might explain the different responses of DBE-containing genes upon RIS depolarization changes. Genes that were differentially regulated during larval starvation were slightly anti-correlated with the genes regulated by *RIS::twk-18gf* and were positively correlated with the genes regulated by *RIS::unc-58gf(strong)* (Figures 3D and 3E). Intestine, muscle, and hypodermis were the tissues most strongly affected by RIS polarization (Data S5). These results indicate that RIS depolarization broadly controls gene expression during L1 arrest, with hyperpolarization of RIS inhibiting gene expression and RIS depolarization promoting gene expression.

We next looked at DAF-16 and PQM-1-associated gene expression in the RIS polarization strains. RIS hyperpolarization reduced DAF-16-associated gene expression as well

(C) Gene set enrichment analysis for DAF-16-related genes shows significant down-regulation of DBE-containing and DAF-16-bound genes, whereas DAE-containing and PQM-1-bound genes are significantly up-regulated. Statistical significance was assessed by Fisher's exact test with Bonferroni correction for multiple comparisons ***$p_{adj} < 0.001$, n.s., not significant.
(D–F) The expression of DBE/DAF-16-regulated genes is dampened during starvation in *aptf-1(gk794)*. DAF-16 target genes that carry the DBE motif that were tested included (D) *sod-3* (***$p_{adj} < 0.001$ for every time point, three biological replicates, wild type: n = 88, *aptf-1*(gk794): n = 87), (E) *hsp-12.6* (***$p_{adj} < 0.001$ for time > 12 h, one biological replicate, wild type: n = 6, *aptf-1*(gk794): n = 7), and (F) *hil-1* (***$p_{adj} < 0.001$ for every time point, one biological replicate, wild type: n = 18, *aptf-1*(gk794): n = 18). Statistical significance in all cases was assessed with Welch's t test, and the p values were subsequently corrected for multiple comparisons using the Benjamini-Hochberg method. Error bars denote the standard error of the mean.
Related data can be found in Figure S1, Data S3 and S4, and in GSE196158.

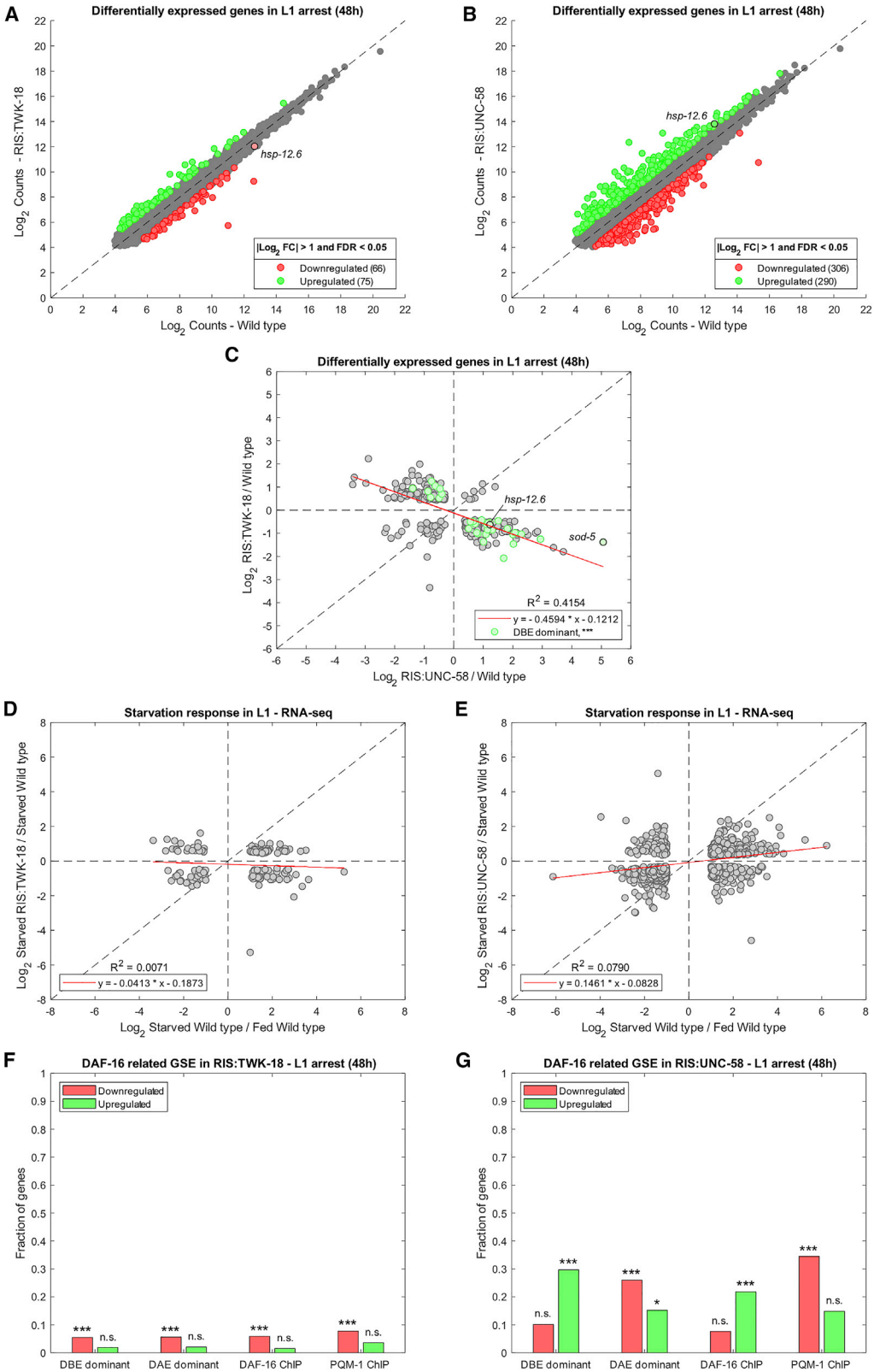

(legend on next page)

as PQM-1-associated gene expression. RIS depolarization increased DAF-16-associated gene expression but rather decreased PQM-1 associated gene expression (Figures 3G and 3H). These results indicate that RIS polarization levels control DAF-16-associated gene expression during the arrest.

RIS depolarization promotes DAF-16/FOXO activation

Our transcriptome analysis indicated that genes that contain the DBE and are bound by DAF-16 are controlled by RIS polarization levels. This suggested that RIS depolarization might directly control DAF-16 activity. To test this hypothesis and to directly test whether DAF-16 is active during sleep or wakefulness, we monitored the nuclear localization of this transcription factor in dependence of the levels of RIS depolarization. We first scored DAF-16::GFP localization and quantified sleep by monitoring animals inside microfluidic devices with a high time resolution.[44,45] DAF-16 was highly dynamic, and its localization changed rapidly between nuclear and cytosolic phases with each phase lasting from a few minutes up to about 2 h. The nuclear or cytoplasmic localization of DAF-16 changed systemically across the major tissues in which DAF-16 was visible (i.e., it was either nuclear or cytoplasmic simultaneously in several tissues including the intestine, hypodermis, and neurons). The animals went through bouts of sleep that could be detected as phases of immobility. These sleep bouts were typically much shorter than phases of nuclear DAF-16, and there was no apparent direct correlation between the behavioral state of the animal and DAF-16 localization (Figures 4A–4D). *aptf-1(gk794)* caused a significant increase in cytoplasmic DAF-16, which appeared to be caused by an increase in long phases of cytoplasmic DAF-16, and a decrease in nuclear DAF-16 (Figure 4B). This analysis indicates that DAF-16 activation is highly fluctuating and that RIS supports DAF-16 activation. As DAF-16 activation transients can occur both during sleep and wake phases, this suggests that RIS exerts a highly indirect and long-lasting effect on DAF-16 that could affect the physiology broadly during both sleep and wakefulness.

We next monitored the nuclear localization of DAF-16::GFP over several days, but with lower time resolution in three strains in which RIS was manipulated: (1) in *aptf-1(gk794)*, in which RIS is dysfunctional; (2) in the *RIS::twk-18gf* strain, in which RIS is hyperpolarized; and (3) in the *RIS::unc-58gf(strong)* strain, in which RIS is depolarized. *aptf-1(gk794)* and *RIS::twk-18gf* caused a reduction in DAF-16::GFP nuclear localization, an effect that was most prominent after 2 days of starvation. In *RIS::unc-58gf(strong)*, the nuclear fraction was increased strongly compared with the wild type on the first day of starvation, and then declined (Figure 4C; Data S6). Thus, RIS depolarization levels appear to be able to affect DAF-16 activation levels at least during some time points during the arrest.

The effects of RIS depolarization on DAF-16 activation suggest that RIS might promote survival through *daf-16*-dependent gene expression. We hence tested the effects of *daf-16* deletion on survival when RIS is impaired or overactivated. For this experiment, we combined *daf-16(mu86)* with either *aptf-1(gk794)*, *RIS::twk-18gf* or *RIS::unc-58gf(strong)* and measured the survival during L1 arrest. RIS hyperpolarization and *aptf-1(gk794)* reduced the survival rate during L1 arrest by 47%. *daf-16(mu86)* reduced survival in an otherwise wild-type background by 77%. In an *aptf-1(gk794)* background, *daf-16(mu86)* reduced survival by only 17%. This indicated that *daf-16(mu86)* reduced the rate constant of aging[46] less in the *aptf-1(gk794)* background, supporting the view that *aptf-1* and *daf-16* act in overlapping pathways. *RIS::unc-58gf(strong)*, by contrast, caused an increase of survival of 9% in a wild-type background, but a statistically significant increase of survival could not be detected in the *daf-16(mu86)* background (Figure 4D; Data S7). Additional protective gene expression systems might also be under the control of RIS, which might explain the broad transcriptional changes and the partial phenotypes observed in *daf-16(mu86)*. Together, these results support the idea that RIS promotes lifespan through protective gene expression that requires the activation of DAF-16.

RIS depolarization promotes DAF-16/FOXO-dependent HSP-12.6 expression to support survival

The transcriptome analysis suggested that RIS depolarization promotes the expression of DBE/DAF-16-dependent genes whose transcription is increased during L1 arrest. These genes include chaperones such as HSP-12.6 that might increase lifespan during starvation. We thus first tested whether RIS depolarization controls the expression of HSP-12.6. For this experiment, we quantified the endogenous HSP-12.6 tagged with an mKate2 fluorescent transgene in the strains in which RIS was hyperpolarized or constantly depolarized. Hyperpolarization of RIS dampened the induction of HSP-12.6::mKate2 expression during L1 arrest, whereas depolarization of RIS increased the expression of HSP-12.6::mKate2 compared with wild-type animals (Figure 5A).

HSP-12.6 has been shown to extend lifespan in the adult.[38] To test if HSP-12.6 also extends survival during L1 arrest and

Figure 3. RIS depolarization promotes gene expression including the expression of DAF-16 target genes

(A and B) Scatterplot overview of RNA-seq data of (A) *RIS::twk-18gf* versus wild type and (B) *RIS::unc-58gf(strong)* versus wild type. Statistically not significant entries according to the selected thresholds are marked in gray. *hsp-12.6* was consistently down- (Log_2 FC = −0.62) and up-regulated (Log_2 FC = 1.22) in *RIS::twk-18gf* and *RIS::unc-58gf(strong)*, respectively.

(C) Comparison of gene expression in the constantly hyperpolarized strain versus the constantly depolarized strain shows an anti-correlated expression pattern. DBE-dominant gene expression was anti-correlated in *RIS::twk-18gf* vs *RIS::unc-58gf(strong)* with the majority of genes down-regulated in *RIS::twk-18gf* and up-regulated in *RIS::unc-58gf(strong)*. This RIS-controlled gene set is enriched for DBE-containing genes (Fisher's exact test, ***$p < 0.001$).

(D and E) Scatterplot overview of RNA-seq data of (D) *RIS::twk-18gf* and (E) *RIS::unc-58gf(strong)* versus genes that are differentially expressed during the starvation response indicates that *RIS::twk-18gf* dampens and *RIS::unc-58gf(strong)* supports the starvation gene expression response.

(F) Gene set enrichment analysis in *RIS::twk-18gf* for DAF-16-related genes shows significant down-regulation of DBE-containing and DAF-16-bound genes, as well as DAE-containing and PQM-1-bound genes.

(G) Gene set enrichment analysis in *RIS::unc-58gf(strong)* for DAF-16-related genes shows significant up-regulation of DBE-containing and DAF-16-bound genes, as well as a mostly down-regulation of DAE-containing and PQM-1-bound genes. Statistical significance was assessed by Fisher's exact test with Bonferroni correction for multiple comparisons, *$p_{adj} < 0.05$, ***$p_{adj} < 0.001$, n.s., not significant.

Related data can be found in Figure S2, Data S5, and in GSE196380.

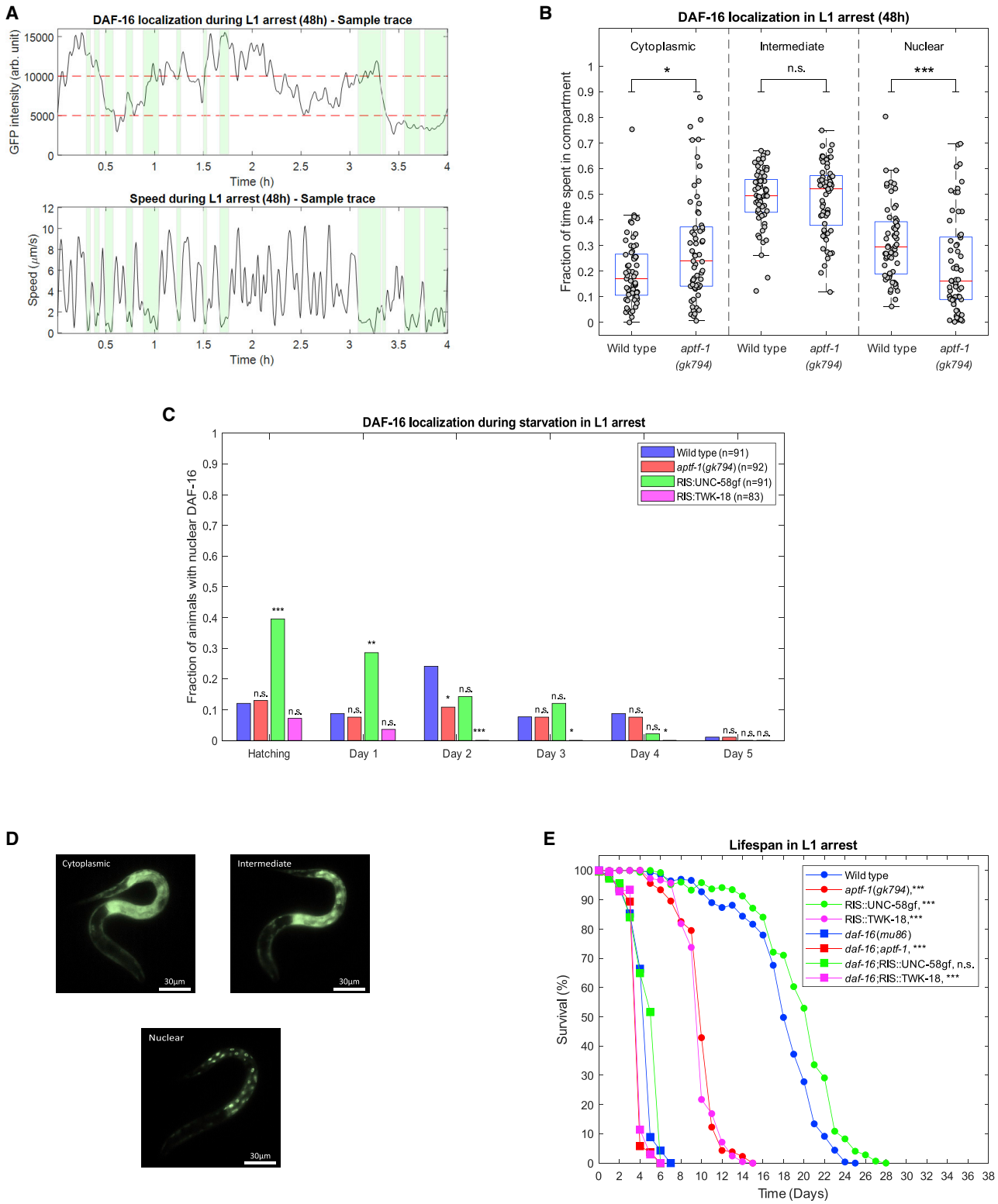

Figure 4. RIS depolarization promotes DAF-16/FOXO activation

(A) DAF-16::GFP localization is highly dynamic and variable. A representative sample trace (n = 1) of sleep bouts (green) detected by motion speed. DAF-16 localization was scored as mostly nuclear, intermediate, or cytoplasmic (red dashed line) during L1 arrest. Nuclear DAF-16::GFP did not correlate visibly with sleep bouts. DAF-16 localization was assessed, using a custom-made MATLAB script, depending on the total nuclear GFP intensity as follows: GFP < 5,000 "Cytoplasmic"; 5,000 < GFP < 10,000 "Intermediate"; and GFP > 10,000 "Nuclear."

(legend continued on next page)

whether *hsp-12.6* acts in the same genetic pathway as *aptf-1*, we performed survival experiments. Knockout of *hsp-12.6* reduced the survival by about 3 days, but it did not further reduce survival in an *aptf-1(gk794)* background (Figure 5B; Data S7). These results indicate that HSP-12.6 is an important determinant of arrest survival and that this heat-shock factor acts in the same pathway as RIS. Thus, DBE-dependent gene expression during L1 arrest is a function of RIS depolarization. As the DAF-16 effector HSP-12.6 accounts for only a part of the survival effects, it appears that RIS depolarization promotes survival through the combined increased expression of multiple effectors.

Our results suggested that RIS depolarization controls *hsp-12.6* expression, which depends on *daf-16*. We hence tested directly whether the expression control of *hsp-12.6* by RIS depended on *daf-16*. We measured HSP-12.6 expression in strains in which RIS was impaired or overactivated in a *daf-16(mu86)* background. HSP-12.6 expression was suppressed in all conditions including overactivation of RIS (Figure 5C). These results indicate that DAF-16-dependent expression of HSP-12.6 acts downstream of RIS depolarization.

DAF-16/FOXO is regulated by upstream regulatory pathways that include IIS signaling. We hence tested how RIS interacts with known DAF-16 regulators to control HSP-12.6 expression and to extend survival. The interactors that we tested were DAF-2 (IIS receptor), JKK-1 (JUN kinase kinase), AAK-1/2 (AMPK), FKH-9 (forkhead transcription factor), and HSF-1 (heat-shock factor), all known regulators of DAF-16.[38,47,48] The results suggested that RIS acts downstream of or in parallel to DAF-2, JUN signaling, and AMPK (Figure S3). RIS acts in the same pathway as HSF-1 for HSP-12.6 expression and also survival, suggesting that DAF-16/HSF-1 define a transcriptional program that requires RIS for HSP-12.6 expression[38] (Figure S4).

RIS boosts protective gene expression when sleep is disturbed

Disturbing *C. elegans* during sleep has been shown to cause the activation of several stress response factors, including DAF-16, that promote protective gene expression.[6,49,50] The underlying mechanisms by which protective gene expression is triggered however are unknown. One possible underlying mechanism could be that loss of sleep causes cellular stress, which in turn promotes protective cellular responses. Our gene expression analysis, however, indicates that loss of sleep caused by impairing RIS does not increase but rather reduces stress responses and protective gene expression. Consistent with this finding, RIS depolarization promotes protective gene expression. Our analysis thus rather suggests that the protective response could be promoted by the activation of sleep-active neurons. Across species, sleep neuron activity is under homeostatic control, and disturbing sleep by sensory stimulation is typically followed by increased activation of sleep-active neurons.[11,12] During phases of increased sleep propensity in *C. elegans*, gentle mechanical stimulation typically causes a brief locomotion arousal response that is followed by RIS rebound activation and a phase of increased behavioral quiescence.[12,50–52] Above we show that depolarization of the sleep-active RIS neuron promotes protective gene expression. Together, this suggests that disturbing sleep increases RIS depolarization, which promotes protective gene expression.

To directly probe this hypothesis, we tested whether disturbing sleep during L1 arrest by mechanical stimulation activates DAF-16 and increases expression of HSP-12.6. We applied an established sleep deprivation protocol during which a train of mechanical tapping stimuli is delivered to the animals every 5 min.[49,51] To test whether this stimulus protocol increases RIS activation, we followed RIS activity with calcium imaging during the experiment. To monitor the effects of starvation on the RIS response to tapping, we first tested larvae directly after hatching, when the starvation response is not yet fully mounted and larvae do not yet sleep much. We tested the larvae again 48 h after starvation onset, when sleep is increased.[28,29] In newly hatched larvae, mechanical stimulation directly triggered a small RIS calcium transient (Figure 6A). In 2-day-starved larvae, the RIS calcium transient response to mechanical stimulation was stronger compared with newly hatched larvae. The RIS calcium transient (~20 s) coincided with a phase of slightly increased quiescence. Approximately 60 s after delivery of the stimulus, RIS calcium activity was reduced and quiescence was slightly decreased compared with the baseline (Figure 6B). These observations are consistent with previous studies that demonstrated a role of RIS in quiescence induction and its homeostasis.[12,50,52] Thus, mechanical stimulation during arrest caused a complex RIS activity and behavioral response, consisting of a direct RIS calcium transient and a short period of increased behavioral quiescence, which is then followed by a phase of decreased RIS activity and quiescence. The stimulation-induced RIS activation transients could hypothetically promote protective gene expression, whereas the overall quiescence appears to be reduced upon stimulation.

(B) *aptf-1(gk794)* enhances cytoplasmic localization of DAF-16::GFP ($p = 0.0364$) and decreases nuclear localization ($p = 0.0006$) after 2 days of starvation (Welch's t test). Nuclear DAF-16::GFP did not correlate directly with sleep bouts ($r_s = 0.20405$, n = 61). Wild type (n = 61), *aptf-1(gk794)* (n = 61). The experiment was performed in two biological replicates.

(C) RIS depolarization levels control DAF-16 localization (the experiment was performed in three biological replicates, statistical significance was assessed by Fisher's exact test with Bonferroni correction for multiple comparisons, $^{***}p_{adj} < 0.001$, $^{**}p_{adj} < 0.01$, $^{*}p_{adj} < 0.05$, n.s., not significant; wild type: n = 91, *aptf-1*(gk794): n = 92, *RIS::unc-58gf*: n = 91, *RIS::twk-18gf*: n = 83).

(D) Sample images of cytoplasmic, intermediate, and nuclear DAF-16::GFP. DAF-16::GFP typically displayed systemic changes in localization.

(E) Constant RIS depolarization increased the median survival span by 8.7% in L1 arrest (wild type = 18.25 days, *RIS::unc-58gf(strong)* = 19.85 days, *daf-16(mu86)* = 4.20 days, *daf-16*; *RIS::unc-58gf(strong)* = 5.1 days). Impairing RIS decreased the median survival span by approximately 47% (wild type = 18.25 days, aptf-*1(gk794)* = 9.70 days, *RIS::twk-18gf* = 9.45 days), whereas in the *daf-16(mu86)* background the 50% survival is decreased only by 16.6% (*daf-16(mu86)* = 4.20 days, *daf-16*; aptf-*1* = 3.5 days, *daf-16*; *RIS::twk-18gf* = 3.5 days). Statistical significance was assessed by Fisher's exact test with Bonferroni correction for multiple comparisons calculated at the time point of 50% survival $^{***}p_{adj} < 0.001$, n.s., not significant. The experiment was performed in three biological replicates with an average number of worms counted per sample per time point as follows: wild type: n > 85, *aptf-1(gk794)*: n > 45, *RIS::unc-58gf*: n > 48, *RIS::-18*: n > 59, *daf-16(mu86)*: n > 64, *daf-16(mu86)*; *aptf-1(gk794)*: n > 38, *daf-16*; *RIS::unc-58gf*: n > 69, *daf-16*; *RIS::twk-18gf*: n > 65.

Related data can be found in Data S6 and S7.

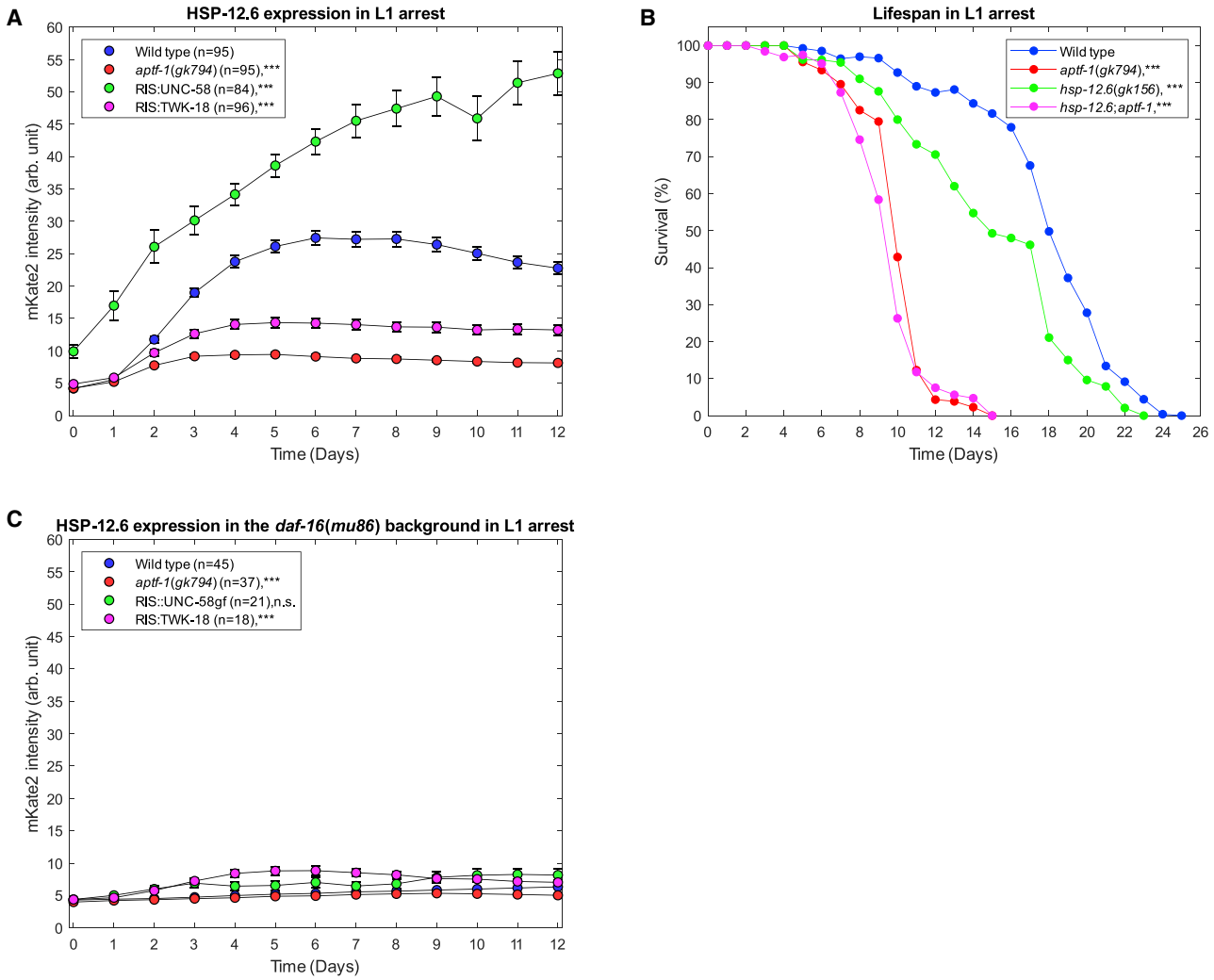

Figure 5. RIS depolarization promotes HSP-12.6 expression through DAF-16/FOXO to promote survival

(A) HSP-12.6 expression depends on RIS depolarization. Statistical significance was assessed by Welch's t test, and the p values were subsequently corrected for multiple comparisons using the Benjamini-Hochberg method, ***$p_{adj} < 0.001$ for time > 2 days; wild type: n = 95, *aptf-1*(gk794): n = 95, *RIS::unc-58gf*: n = 84, *RIS::twk-18*: n = 96. Error bars denote the standard error of the mean.

(B) Deletion of *hsp-12.6* decreases the median survival span by 17% in the wild-type background. Although it does not further reduce the survival in the *aptf-1(gk794)* background (survival spans: wild type = 18.25 days, *hsp-12.6(gk156)* = 15.15 days, aptf-*1(gk794)* = 9.70 days, *hsp-12.6(gk156)*; aptf-*1(gk794)* = 9.15 days, wild-type and *aptf-1* data are the same as in Figure 4E). Statistical significance was assessed by Fisher's exact test with Bonferroni correction for multiple comparisons calculated for the median survival span ***$p_{adj} < 0.001$. The experiment was performed in three biological replicates with an average number of worms counted per sample per time point as follows: wild-type: n > 85, *aptf-1(gk794)*: n > 45, *hsp-12.6(gk156)*: n > 66, *hsp-12.6(gk156)*; *aptf-1(gk794)*: n > 74.

(C) HSP-12.6 expression is suppressed in all conditions in the *daf-16(mu86)* background, suggesting that DAF-16 acts downstream of RIS. Statistical significance was assessed by Welch's t test, and the p values were subsequently corrected for multiple comparisons using the Benjamini-Hochberg method ***$p_{adj} < 0.001$, n.s.: not significant for time > 2 days; wild type: n = 45, *aptf-1*(gk794): n = 37, *RIS::unc-58gf*: n = 21, *RIS::twk-18*: n = 18. Error bars denote the standard error of the mean.

Related data can be found in Figures S3 and S4 and Data S7.

To test whether RIS activation following mechanical stimulation is caused by sensory perception, e.g., through perception by touch sensory neurons, we repeated the RIS activity measurements in a mutant, *mec-4(u253)*, which lacks responsiveness of sensory neurons to gentle mechanical stimulation.[53] RIS calcium activation upon sensory stimulation was abolished in the mechanosensation-defective mutant, indicating that sensory neuron activation promotes RIS activation (Figures 6A and 6B). Hence, RIS activates upon perception of mechanical stimulation. Activation of RIS increased together with the propensity of larvae to sleep. This effect was similar to RIS activation in developing larvae that show little RIS activation upon mechanical stimulation during the intermolt when they are constantly active, but they show increased RIS responsiveness to mechanical stimulation during lethargus, when sleep bouts occur.[12,29,51] RIS is activated by locomotion-controlling circuits at the transition from forward to reverse movement,[12,20,21] suggesting that mechanical stimulation might cause activation of RIS through arousal of locomotion circuits.

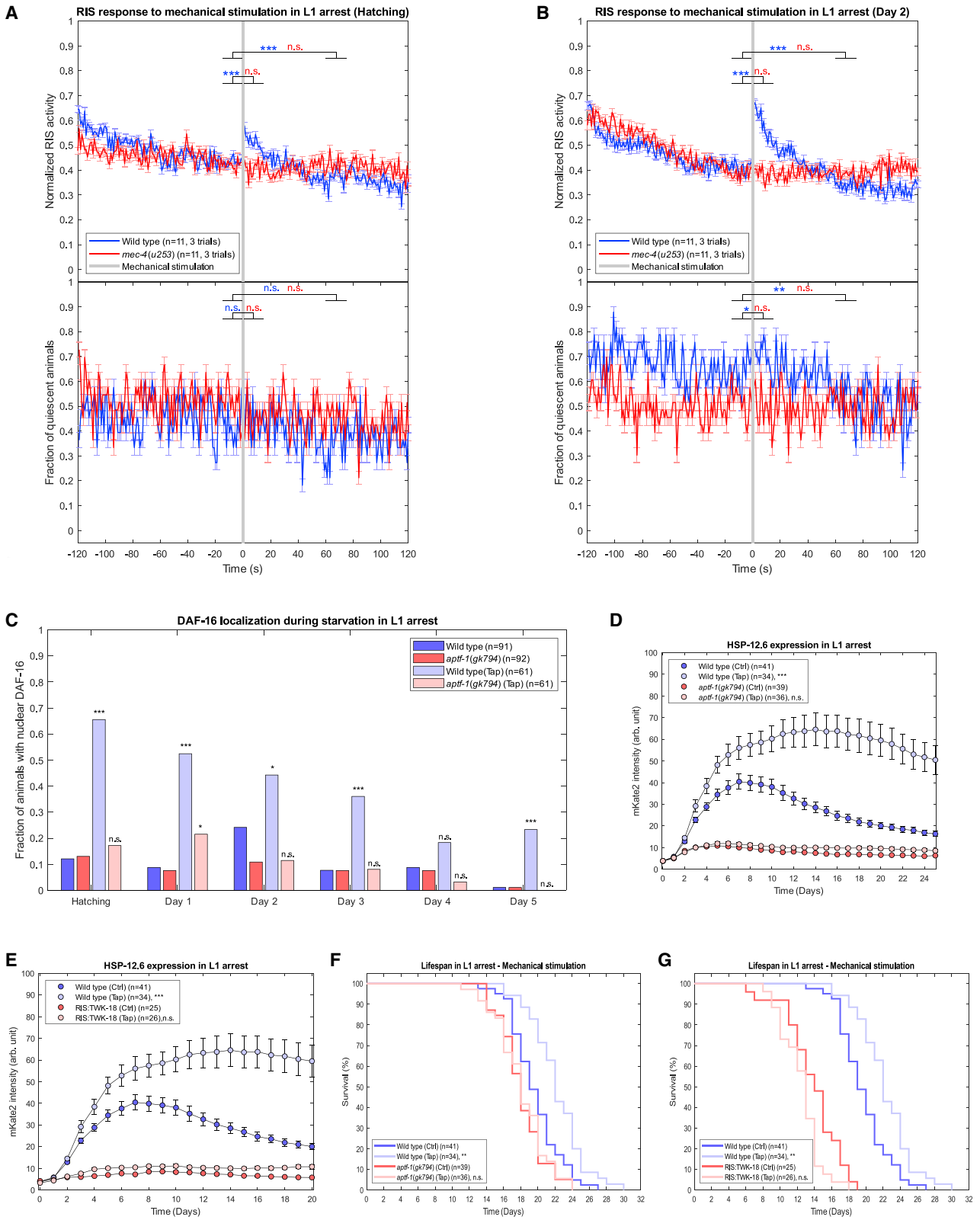

Figure 6. RIS promotes protective gene expression when sleep is disturbed

(A and B) Mechanical stimulation that is applied to disturb the animal during sleep increases RIS activity in L1 arrest. (A) Tapping performed at hatching (day 0) results in a small RIS activation. (B) Tapping performed after 2 days of starvation results in a stronger RIS activation. Statistical significance of the effect of tapping

(legend continued on next page)

We then applied the sensory stimulation protocol for several days and followed DAF-16::GFP localization. Consistent with previous reports,[6,49] mechanical stimulation increased the fraction of nuclear DAF-16 during most time points (Figure 6C). To test whether the increased activation of DAF-16 depends on RIS, we tested the effects of the sleep deprivation protocol on *aptf-1(gk794)* animals. The effect of sensory stimulation on DAF-16 localization was always stronger in a wild-type background compared with *aptf-1(gk794)*. We next tested whether sensory stimulation also increased HSP-12.6::mKate2 expression. Indeed, sensory stimulation substantially increased the expression of HSP-12.6, and HSP-12.6 expression was fully dependent on *aptf-1* and RIS depolarization (Figures 6D and 6E), as well as *mec-4* (Figure S5A). Hence, mechanical disturbance increases protective gene expression through RIS.

The increased protective gene expression that results from the sleep deprivation protocol might increase starvation resistance. To test this idea, we measured the starvation resistance of larvae that were subjected to the sleep disturbance protocol. Sleep disturbance increased the lifespan by about 3 days in wild-type animals but did not increase survival in *aptf-1(gk794)* and *RIS::twk-18gf*, indicating that mechanical stimulation increases survival through RIS (Figures 6F and 6G). Lifespan extension by mechanical stimulation also fully depended on *mec-4* and thus again on sensory perception of the stimulus (Figure S5B). These experiments indicate that protective gene expression and DAF-16 activation are promoted through activation of the RIS neuron when the animal is disturbed by mechanosensory stimulation. Other stimuli such as blue light or temperature elevation have also been shown to cause RIS activation, either directly or as a rebound activation following RIS inhibition.[12,39,51,54,55] This suggests that RIS activation may play a protective role in the context of multiple sensory responses. Together, our data suggest a model in which sleep deprivation promotes protective gene expression through the depolarization of RIS.

DISCUSSION

Sensory stimulation of sleeping worms activates FOXO,[6,49] which increases subsequent sleep[50,56] and supports survival.[6] We previously showed that during L1 arrest, FOXO/DAF-16 together with AMP-activated kinase AAK-1/2 promotes RIS activation to increase sleep.[29] Hence, FOXO acts both as an upstream promoter of sleep as well as a response factor downstream of sleep. Nonetheless, how does sleep deprivation cause the activation of stress response pathways, such as the activation of FOXO?[6,49] An obvious explanation would be that the sleep deprivation procedure is stressful per se and thus triggers stress responses.[13,14] As an alternative explanation, the absence of sleep or increased wakefulness could impair an essential function, thus causing cellular stress and a subsequent cellular stress response.[5,15] Our gene expression analysis, however, did not detect increased stress responses following impairment of RIS but instead found increased stress response gene expression when RIS is activated. Thus, surprisingly, our data do not support a model in which the activation of FOXO and stress response gene expression is generated by broad cellular stress caused by the loss of sleep or increased wakefulness.

Our transcription analysis rather supports a third model in which gene expression is promoted by the depolarization of RIS. We show that RIS impairment blunts protective gene expression, whereas activation of RIS increases it. These results show that RIS depolarization levels positively modulate the gene expression response. While RIS typically depolarizes during sleep, the effects on gene expression do not seem to be restricted to sleep bouts but also extend to wake phases.

Sleep disturbance by mechanical stimulation induces brief additional RIS activation transients but also a subsequent phase of reduced quiescence. How altered RIS depolarization and quiescence patterns contribute to gene expression during sleep disturbance is, however, impossible to deduce from such sleep disturbance protocols. This question can be better addressed by direct manipulations of RIS depolarization. Interestingly, both hyperpolarization (*RIS::twk-18gf*) as well as constant depolarization (*RIS::unc-58gf(strong)*) of RIS abolish most sleep behavior.[41] The use of these RIS depolarization mutants hence allowed us to test specifically for the effects of RIS depolarization independently of sleep.[41] As hyperpolarization of RIS inhibits and constant depolarization of RIS promotes protective gene expression during L1 arrest, these gene expression changes appear to be functions of RIS polarization rather than sleep and behavioral quiescence. A plausible interpretation of the sleep disturbance assay could thus be that the stimulation-induced RIS calcium transients promote protective gene expression independently of quiescence.

was assessed by Wilcoxon signed-rank test with Bonferroni correction for multiple comparisons *$p_{adj} < 0.05$, **$p_{adj} < 0.01$, n = 18; each animal was probed with three trials, which were averaged. Wild type: n = 11, *mec-4*(u253): n = 11, one biological replicate.

(C) DAF-16 localization after mechanical stimulation, depends on RIS. The experiment was performed in two biological replicates. Statistical significance of the effect of tapping was assessed by two-way ANOVA, with correction for multiple comparisons using Tukey's honest significant difference criterion **$p_{adj} < 0.01$, *$p_{adj} < 0.05$, n.s., not significant; wild type (ctrl): n = 91, *aptf-1*(gk794) (ctrl): n = 92; wild type (tap): n = 61, *aptf-1*(gk794) (tap): n = 61. Control and *aptf-1(-)* data without tapping are the same as in Figure 3.

(D and E) Mechanical stimulation increases the expression of HSP-12.6 in a RIS-dependent manner. (D) RIS impairment with *aptf-1*(gk794) and (E) RIS impairment with *RIS::twk-18gf*. The experiment was performed in two biological replicates. Statistical significance of the effect of tapping was assessed by Welch's t test, and the p values were subsequently corrected for multiple comparisons using the Benjamini-Hochberg method ***$p_{adj} < 0.001$ for time > 2 days. Wild type (ctrl): n = 41, wild type (tap): n = 34; *aptf-1*(gk794) (ctrl): n = 39, *aptf-1*(gk794) (tap): n = 36; *RIS::twk-18gf* (ctrl): n = 25, *RIS::twk-18gf* (tap): n = 26. The same wild-type data are used for (D) and (E). Error bars denote the standard error of the mean.

(F and G) Mechanical stimulation increases the lifespan in L1 arrest in a RIS-dependent manner. (F) RIS impairment with *aptf-1*(gk794) and (G) RIS impairment with *RIS::twk-18gf*. Mechanical stimulation increases the 50% survival by 13.3% in L1 arrest (wild type [ctrl] = 19.20 days, wild type [tap] = 21.76 days) and in a RIS-dependent manner (*aptf-1(gk794)* [ctrl] = 17.5 days, *aptf-1(gk794)* [tap] = 17.5 days; *RIS::twk-18gf* [ctrl] = 14 days, *RIS::twk-18gf* [tap] = 13 days). The experiment was performed in two biological replicates. Statistical significance of the effect of tapping was assessed by the log-rank test **$p < 0.01$, n.s., not significant. Wild type (ctrl): n = 41, wild type (tap): n = 35; *aptf-1*(gk794) (ctrl): n = 39, *aptf-1*(gk794) (tap): n = 35; *RIS::twk-18gf* (ctrl): n = 25, *RIS::twk-18gf* (tap): n = 26. The same wild-type data are used for (D) and (E). (F)–(G) were measured in the same animals as (D)–(E).

Related data can be found in Figure S5 and Data S7.

This activation of stress response gene expression through RIS ultimately promotes starvation resistance. We hence showed that disturbing sleep can provide organismic benefits by positively modulating a protective gene expression stress response.

More generally, these results suggest that sleep-active neuron depolarization might also account for increased gene expression changes in the context of cellular stress responses in other species, including in humans. The gene expression changes underlying stress response pathways can mitigate but also mediate effects of sleep deprivation.[49] A stress response mounted by the overactivation of sleep-active neurons in the context of sleep deprivation could thus even have beneficial effects. On the other hand, chronically overactivated stress responses can be deleterious.[3] Hence, managing the activity of sleep-active neurons will likely become an important intervention to manage health and to treat the consequences of disturbed sleep. For example, inhibition of sleep-active neurons could become a treatment strategy for mitigating adverse effects that are potentially caused by overshooting stress gene expression changes during chronic insomnia.

STAR★METHODS

Detailed methods are provided in the online version of this paper and include the following:

- KEY RESOURCES TABLE
- RESOURCE AVAILABILITY
  - Lead contact
  - Materials availability
  - Data and code availability
- EXPERIMENTAL MODEL AND SUBJECT DETAILS
- METHOD DETAILS
  - Generation of transgenic knock-in using CRISPR
  - Transcriptional profiling by RNA-sequencing
  - Sequencing
  - Proteomic characterization of *C. elegans*
  - Survival and lifespan of L1 arrested animals
  - Long-term imaging using agarose hydrogel microchambers
  - Fluorescence imaging in L1 arrest
  - Heat shock
  - GCaMP imaging
  - Mechanical stimulation
  - Quantification of DAF-16::GFP nuclear localization
- QUANTIFICATION AND STATISTICAL ANALYSIS
  - Transcriptional profiling by RNA-sequencing and GSE analysis
  - Proteomic characterization of *C. elegans*
  - Survival and lifespan of L1 arrested animals
  - Fluorescence imaging in L1 arrest
  - GCaMP imaging
  - Mechanical stimulation
  - Quantification of DAF-16::GFP nuclear localization

SUPPLEMENTAL INFORMATION

Supplemental information can be found online at https://doi.org/10.1016/j.cub.2022.04.012.

ACKNOWLEDGMENTS

We thank the *Caenorhabditis* Genetics Center supported by the National Institutes of Health Office of Research Infrastructure Programs (P40 OD010440) for strains. We thank Eva Naumann and Diana Omarova for assisting in the creation and maintenance of some of the strains used in this study and Monika Raabe and Uwe Plessmann for technical support with MS measurements. Jik Nijssen helped with bioinformatics analysis. This work was supported by a European Research Council Starting Grant (ID: 637860, SLEEPCONTROL) to H.B. and a grant from the Deutsche Forschungsgemeinschaft (SPP1935) to H.U.

AUTHOR CONTRIBUTIONS

A.K. executed and analyzed all of the *C. elegans* experiments, prepared the figures, and edited the paper. L.M.W., A.W., and H.U. generated the TMT proteome data. D.M. generated the LFQ proteome data. S.B. and B.T. generated transcriptome data. I.B. generated the samples for the transcriptomes of the RIS polarization mutants. H.B. conceived the study and experiments, acquired funding, supervised the project, and wrote the paper. All authors agreed to the final version of the manuscript.

DECLARATION OF INTERESTS

The authors declare no competing interests.

Received: August 19, 2021
Revised: February 9, 2022
Accepted: April 6, 2022
Published: May 2, 2022

REFERENCES

1. Cirelli, C., Gutierrez, C.M., and Tononi, G. (2004). Extensive and divergent effects of sleep and wakefulness on brain gene expression. Neuron *41*, 35–43.
2. Mackiewicz, M., Shockley, K.R., Romer, M.A., Galante, R.J., Zimmerman, J.E., Naidoo, N., Baldwin, D.A., Jensen, S.T., Churchill, G.A., and Pack, A.I. (2007). Macromolecule biosynthesis: a key function of sleep. Physiol. Genomics *31*, 441–457. https://doi.org/10.1152/physiolgenomics.00275.2006.
3. Meerlo, P., Sgoifo, A., and Suchecki, D. (2008). Restricted and disrupted sleep: effects on autonomic function, neuroendocrine stress systems and stress responsivity. Sleep Med. Rev. *12*, 197–210. https://doi.org/10.1016/j.smrv.2007.07.007.
4. Naidoo, N., Giang, W., Galante, R.J., and Pack, A.I. (2005). Sleep deprivation induces the unfolded protein response in mouse cerebral cortex. J. Neurochem. *92*, 1150–1157. https://doi.org/10.1111/j.1471-4159.2004.02952.x.
5. Williams, J.A., and Naidoo, N. (2020). Sleep and cellular stress. Curr. Opin. Physiol. *15*, 104–110. https://doi.org/10.1016/j.cophys.2019.12.011.
6. Driver, R.J., Lamb, A.L., Wyner, A.J., and Raizen, D.M. (2013). DAF-16/FOXO regulates homeostasis of essential sleep-like behavior during larval transitions in *C. elegans*. Curr. Biol. *23*, 501–506. https://doi.org/10.1016/j.cub.2013.02.009.
7. Xia, M., Li, Z., Li, S., Liang, S., Li, X., Chen, B., Zhang, M., Dong, C., Verkhratsky, A., Guan, D., and Li, B. (2020). Sleep deprivation selectively down-regulates astrocytic 5-HT2B receptors and triggers depressive-like behaviors via stimulating P2X7 receptors in mice. Neurosci. Bull. *36*, 1259–1270. https://doi.org/10.1007/s12264-020-00524-4.
8. Shaw, P.J., Tononi, G., Greenspan, R.J., and Robinson, D.F. (2002). Stress response genes protect against lethal effects of sleep deprivation in *Drosophila*. Nature *417*, 287–291. https://doi.org/10.1038/417287a.
9. Saper, C.B., Fuller, P.M., Pedersen, N.P., Lu, J., and Scammell, T.E. (2010). Sleep state switching. Neuron *68*, 1023–1042. https://doi.org/10.1016/j.neuron.2010.11.032.

10. Bringmann, H. (2018). Sleep-active neurons: conserved motors of sleep. Genetics *208*, 1279–1289. https://doi.org/10.1534/genetics.117.300521.

11. Alam, M.A., Kumar, S., McGinty, D., Alam, M.N., and Szymusiak, R. (2014). Neuronal activity in the preoptic hypothalamus during sleep deprivation and recovery sleep. J. Neurophysiol. *111*, 287–299. https://doi.org/10.1152/jn.00504.2013.

12. Maluck, E., Busack, I., Besseling, J., Masurat, F., Turek, M., Busch, K.E., and Bringmann, H. (2020). A wake-active locomotion circuit depolarizes a sleep-active neuron to switch on sleep. PLoS Biol. *18*, e3000361. https://doi.org/10.1371/journal.pbio.3000361.

13. Meerlo, P., Koehl, M., van der Borght, K., and Turek, F.W. (2002). Sleep restriction alters the hypothalamic-pituitary-adrenal response to stress. J. Neuroendocrinol. *14*, 397–402.

14. Chrousos, G., Vgontzas, A.N., and Kritikou, I. (2016). HPA axis and sleep. In Endotext, L.J. De Groot, G. Chrousos, K. Dungan, K.R. Feingold, A. Grossman, J.M. Hershman, C. Koch, M. Korbonits, and R. McLachlan, et al., eds. Endotext.org.

15. Allada, R., and Siegel, J.M. (2008). Unearthing the phylogenetic roots of sleep. Curr. Biol. *18*, R670–R679. https://doi.org/10.1016/j.cub.2008.06.033.

16. Bringmann, H. (2019). Genetic sleep deprivation: using sleep mutants to study sleep functions. EMBO Rep. *20*, e46807. https://doi.org/10.15252/embr.201846807.

17. Krause, A.J., Simon, E.B., Mander, B.A., Greer, S.M., Saletin, J.M., Goldstein-Piekarski, A.N., and Walker, M.P. (2017). The sleep-deprived human brain. Nat. Rev. Neurosci. *18*, 404–418. https://doi.org/10.1038/nrn.2017.55.

18. Turek, M., Lewandrowski, I., and Bringmann, H. (2013). An AP2 transcription factor is required for a sleep-active neuron to induce sleep-like quiescence in *C. elegans*. Curr. Biol. *23*, 2215–2223. https://doi.org/10.1016/j.cub.2013.09.028.

19. Turek, M., Besseling, J., Spies, J.P., König, S., and Bringmann, H. (2016). Sleep-active neuron specification and sleep induction require FLP-11 neuropeptides to systemically induce sleep. eLife *5*, e12499. https://doi.org/10.7554/eLife.12499.

20. Steuer Costa, W., Van der Auwera, P., Glock, C., Liewald, J.F., Bach, M., Schüler, C., Wabnig, S., Oranth, A., Masurat, F., Bringmann, H., et al. (2019). A GABAergic and peptidergic sleep neuron as a locomotion stop neuron with compartmentalized Ca2+ dynamics. Nat. Commun. *10*, 4095. https://doi.org/10.1038/s41467-019-12098-5.

21. Nichols, A.L.A., Eichler, T., Latham, R., and Zimmer, M. (2017). A global brain state underlies *C. elegans* sleep behavior. Science *356*, eaam6851. https://doi.org/10.1126/science.aam6851.

22. Van Buskirk, C., and Sternberg, P.W. (2007). Epidermal growth factor signaling induces behavioral quiescence in *Caenorhabditis elegans*. Nat. Neurosci. *10*, 1300–1307. https://doi.org/10.1038/nn1981.

23. Hill, A.J., Mansfield, R., Lopez, J.M., Raizen, D.M., and Van Buskirk, C. (2014). Cellular stress induces a protective sleep-like state in *C. elegans*. Curr. Biol. *24*, 2399–2405. https://doi.org/10.1016/j.cub.2014.08.040.

24. Trojanowski, N.F., Nelson, M.D., Flavell, S.W., Fang-Yen, C., and Raizen, D.M. (2015). Distinct mechanisms underlie quiescence during two *Caenorhabditis elegans* sleep-like states. J. Neurosci. *35*, 14571–14584. https://doi.org/10.1523/JNEUROSCI.1369-15.2015.

25. Skora, S., Mende, F., and Zimmer, M. (2018). Energy scarcity promotes a brain-wide sleep state modulated by insulin signaling in *C. elegans*. Cell Rep *22*, 953–966. https://doi.org/10.1016/j.celrep.2017.12.091.

26. Sinner, M.P., Masurat, F., Ewbank, J.J., Pujol, N., and Bringmann, H. (2021). Innate immunity promotes sleep through epidermal antimicrobial peptides. Curr. Biol. *31*. 564.e12–577.e12. https://doi.org/10.1016/j.cub.2020.10.076.

27. Baugh, L.R. (2013). To grow or not to grow: nutritional control of development during *Caenorhabditis elegans* L1 arrest. Genetics *194*, 539–555. https://doi.org/10.1534/genetics.113.150847.

28. Baugh, L.R., and Hu, P.J. (2020). Starvation responses throughout the *Caenorhabditis elegans* life cycle. Genetics *216*, 837–878. https://doi.org/10.1534/genetics.120.303565.

29. Wu, Y., Masurat, F., Preis, J., and Bringmann, H. (2018). Sleep counteracts aging phenotypes to survive starvation-induced developmental arrest in *C. elegans*. Curr. Biol. *28*. 3610.e8–3624.e8. https://doi.org/10.1016/j.cub.2018.10.009.

30. Baugh, L.R., and Sternberg, P.W. (2006). DAF-16/FOXO regulates transcription of cki-1/Cip/Kip and repression of lin-4 during *C. elegans* L1 arrest. Curr. Biol. *16*, 780–785. https://doi.org/10.1016/j.cub.2006.03.021.

31. Furuyama, T., Nakazawa, T., Nakano, I., and Mori, N. (2000). Identification of the differential distribution patterns of mRNAs and consensus binding sequences for mouse DAF-16 homologues. Biochem. J. *349*, 629–634. https://doi.org/10.1042/0264-6021:3490629.

32. Tepper, R.G., Ashraf, J., Kaletsky, R., Kleemann, G., Murphy, C.T., and Bussemaker, H.J. (2013). PQM-1 complements DAF-16 as a key transcriptional regulator of DAF-2-mediated development and longevity. Cell *154*, 676–690. https://doi.org/10.1016/j.cell.2013.07.006.

33. Hibshman, J.D., Doan, A.E., Moore, B.T., Kaplan, R.E., Hung, A., Webster, A.K., Bhatt, D.P., Chitrakar, R., Hirschey, M.D., and Baugh, L.R. (2017). *daf-16*/FoxO promotes gluconeogenesis and trehalose synthesis during starvation to support survival. eLife *6*, e30057. https://doi.org/10.7554/eLife.30057.

34. Libina, N., Berman, J.R., and Kenyon, C. (2003). Tissue-specific activities of *C. elegans* DAF-16 in the regulation of lifespan. Cell *115*, 489–502.

35. Honjoh, S., Yamamoto, T., Uno, M., and Nishida, E. (2009). Signalling through RHEB-1 mediates intermittent fasting-induced longevity in *C. elegans*. Nature *457*, 726–730. https://doi.org/10.1038/nature07583.

36. Jedrusik, M.A., Vogt, S., Claus, P., and Schulze, E. (2002). A novel linker histone-like protein is associated with cytoplasmic filaments in *Caenorhabditis elegans*. J. Cell Sci. *115*, 2881–2891.

37. Harvald, E.B., Sprenger, R.R., Dall, K.B., Ejsing, C.S., Nielsen, R., Mandrup, S., Murillo, A.B., Larance, M., Gartner, A., Lamond, A.I., and Færgeman, N.J. (2017). Multi-omics analyses of starvation responses reveal a central role for lipoprotein metabolism in acute starvation survival in *C. elegans*. Cell Syst *5*. 38.e4–52.e4. https://doi.org/10.1016/j.cels.2017.06.004.

38. Hsu, A.L., Murphy, C.T., and Kenyon, C. (2003). Regulation of aging and age-related disease by DAF-16 and heat-shock factor. Science *300*, 1142–1145. https://doi.org/10.1126/science.1083701.

39. Konietzka, J., Fritz, M., Spiri, S., McWhirter, R., Leha, A., Palumbos, S., Costa, W.S., Oranth, A., Gottschalk, A., Miller, D.M., 3rd., et al. (2020). Epidermal growth factor signaling promotes sleep through a combined series and parallel neural circuit. Curr. Biol. *30*. 1.e13–16.e13. https://doi.org/10.1016/j.cub.2019.10.048.

40. Gonzales, D.L., Zhou, J., Fan, B., and Robinson, J.T. (2019). Microfluidic-induced sleep: a spontaneous *C. elegans* sleep state regulated by satiety, thermosensation and mechanosensation. Preprint at bioRxiv. https://doi.org/10.1101/547075.

41. Busack, I., and Bringmann, H. (2022). Overactivation of a sleep-active neuron decouples survival from the need to sleep. Preprint at bioRxiv. https://doi.org/10.1101/2022.04.03.486914.

42. Taylor, S.R., Santpere, G., Weinreb, A., Barrett, A., Reilly, M.B., Xu, C., Varol, E., Oikonomou, P., Glenwinkel, L., McWhirter, R., et al. (2021). Molecular topography of an entire nervous system. Cell *184*. 4329.e23–4347.e23. https://doi.org/10.1016/j.cell.2021.06.023.

43. Ben Soussia, I., El Mouridi, S., Kang, D., Leclercq-Blondel, A., Khoubza, L., Tardy, P., Zariohi, N., Gendrel, M., Lesage, F., Kim, E.J., et al. (2019). Mutation of a single residue promotes gating of vertebrate and invertebrate two-pore domain potassium channels. Nat. Commun. *10*, 787. https://doi.org/10.1038/s41467-019-08710-3.

44. Bringmann, H. (2011). Agarose hydrogel microcompartments for imaging sleep- and wake-like behavior and nervous system development in

Caenorhabditis elegans larvae. J. Neurosci. Methods *201*, 78–88. https://doi.org/10.1016/j.jneumeth.2011.07.013.

45. Turek, M., Besseling, J., and Bringmann, H. (2015). Agarose microchambers for long-term calcium imaging of *Caenorhabditis elegans*. J. Vis. Exp. e52742. https://doi.org/10.3791/52742.
46. Stroustrup, N., Anthony, W.E., Nash, Z.M., Gowda, V., Gomez, A., López-Moyado, I.F., Apfeld, J., and Fontana, W. (2016). The temporal scaling of *Caenorhabditis elegans* ageing. Nature *530*, 103–107. https://doi.org/10.1038/nature16550.
47. Kaletsky, R., Lakhina, V., Arey, R., Williams, A., Landis, J., Ashraf, J., and Murphy, C.T. (2016). The *C. elegans* adult neuronal IIS/FOXO transcriptome reveals adult phenotype regulators. Nature *529*, 92–96. https://doi.org/10.1038/nature16483.
48. Greer, E.L., Dowlatshahi, D., Banko, M.R., Villen, J., Hoang, K., Blanchard, D., Gygi, S.P., and Brunet, A. (2007). An AMPK-FOXO pathway mediates longevity induced by a novel method of dietary restriction in *C. elegans*. Curr. Biol. *17*, 1646–1656. https://doi.org/10.1016/j.cub.2007.08.047.
49. Sanders, J., Scholz, M., Merutka, I., and Biron, D. (2017). Distinct unfolded protein responses mitigate or mediate effects of nonlethal deprivation of *C. elegans* sleep in different tissues. BMC Biol. *15*, 67. https://doi.org/10.1186/s12915-017-0407-1.
50. Nagy, S., Tramm, N., Sanders, J., Iwanir, S., Shirley, I.A., Levine, E., and Biron, D. (2014). Homeostasis in *C. elegans* sleep is characterized by two behaviorally and genetically distinct mechanisms. eLife *3*, e04380. https://doi.org/10.7554/eLife.04380.
51. Spies, J., and Bringmann, H. (2018). Automated detection and manipulation of sleep in *C. elegans* reveals depolarization of a sleep-active neuron during mechanical stimulation-induced sleep deprivation. Sci. Rep. *8*, 9732. https://doi.org/10.1038/s41598-018-28095-5.
52. McClanahan, P.D., Dubuque, J.M., Kontogiorgos-Heintz, D., Habermeyer, B.F., Xu, J.H., Ma, A.M., Raizen, D.M., and Fang-Yen, C. (2020). A quiescent state following mild sensory arousal in *Caenorhabditis elegans* is potentiated by stress. Sci. Rep. *10*, 4140. https://doi.org/10.1038/s41598-020-60994-4.
53. Suzuki, H., Kerr, R., Bianchi, L., Frøkjaer-Jensen, C., Slone, D., Xue, J., Gerstbrein, B., Driscoll, M., and Schafer, W.R. (2003). In vivo imaging of *C. elegans* mechanosensory neurons demonstrates a specific role for the MEC-4 channel in the process of gentle touch sensation. Neuron *39*, 1005–1017. https://doi.org/10.1016/j.neuron.2003.08.015.
54. Gonzales, D.L., Zhou, J., Fan, B., and Robinson, J.T. (2019). A microfluidic-induced *C. elegans* sleep state. Nat. Commun. *10*, 5035. https://doi.org/10.1038/s41467-019-13008-5.
55. Kotera, I., Tran, N.A., Fu, D., Kim, J.H., Byrne Rodgers, J., and Ryu, W.S. (2016). Pan-neuronal screening in *Caenorhabditis elegans* reveals asymmetric dynamics of AWC neurons is critical for thermal avoidance behavior. eLife *5*, e19021. https://doi.org/10.7554/eLife.19021.
56. Bennett, H.L., Khoruzhik, Y., Hayden, D., Huang, H., Sanders, J., Walsh, M.B., Biron, D., and Hart, A.C. (2018). Normal sleep bouts are not essential for *C. elegans* survival and FoxO is important for compensatory changes in sleep. BMC Neurosci. *19*, 10. https://doi.org/10.1186/s12868-018-0408-1.
57. Lin, K., Hsin, H., Libina, N., and Kenyon, C. (2001). Regulation of the *Caenorhabditis elegans* longevity protein DAF-16 by insulin/IGF-1 and germline signaling. Nat. Genet. *28*, 139–145. https://doi.org/10.1038/88850.
58. elegans Deletion Mutant Consortium, C. (2012). large-scale screening for targeted knockouts in the *Caenorhabditis elegans* genome. G3 (Bethesda) *2*, 1415–1425. https://doi.org/10.1534/g3.112.003830.
59. Brenner, S. (1974). The genetics of *Caenorhabditis elegans*. Genetics *77*, 71–94.
60. Ahringer, J. (2006). Reverse genetics. WormBook. https://doi.org/10.1895/wormbook.1.47.1.
61. Bantscheff, M., Lemeer, S., Savitski, M.M., and Kuster, B. (2012). Quantitative mass spectrometry in proteomics: critical review update from 2007 to the present. Anal. Bioanal. Chem. *404*, 939–965. https://doi.org/10.1007/s00216-012-6203-4.
62. Schwarz, J., Lewandrowski, I., and Bringmann, H. (2011). Reduced activity of a sensory neuron during a sleep-like state in *Caenorhabditis elegans*. Curr. Biol. *21*, R983–R984. https://doi.org/10.1016/j.cub.2011.10.046.
63. Raudvere, U., Kolberg, L., Kuzmin, I., Arak, T., Adler, P., Peterson, H., and Vilo, J. (2019). g:Profiler: a web server for functional enrichment analysis and conversions of gene lists (2019 update). Nucleic Acids Res. *47*, W191–W198. https://doi.org/10.1093/nar/gkz369.
64. Kaletsky, R., Yao, V., Williams, A., Runnels, A.M., Tadych, A., Zhou, S., Troyanskaya, O.G., and Murphy, C.T. (2018). Transcriptome analysis of adult *Caenorhabditis elegans* cells reveals tissue-specific gene and isoform expression. PLoS Genet. *14*, e1007559. https://doi.org/10.1371/journal.pgen.1007559.
65. Han, M., Wei, G., McManus, C.E., Hillier, L.W., and Reinke, V. (2019). Isolated *C. elegans* germ nuclei exhibit distinct genomic profiles of histone modification and gene expression. BMC Genomics *20*, 500. https://doi.org/10.1186/s12864-019-5893-9.
66. Cox, J., Neuhauser, N., Michalski, A., Scheltema, R.A., Olsen, J.V., and Mann, M. (2011). Andromeda: a peptide search engine integrated into the MaxQuant environment. J. Proteome Res. *10*, 1794–1805. https://doi.org/10.1021/pr101065j.
67. Tyanova, S., Temu, T., Sinitcyn, P., Carlson, A., Hein, M.Y., Geiger, T., Mann, M., and Cox, J. (2016). The Perseus computational platform for comprehensive analysis of (prote)omics data. Nat. Methods *13*, 731–740. https://doi.org/10.1038/nmeth.3901.

STAR★METHODS

KEY RESOURCES TABLE

REAGENT or RESOURCE	SOURCE	IDENTIFIER
C. elegans strains		
Wild type	CGC	N2 (Figures 1A, 1C, 1E, 1F, 2A–2C, 3A–3G, 4E, S1A, S3E, S3F, and S4B)
aptf-1(gk794) II.	Turek et al.[18]	HBR227 (Figures 1B, 1D–1F, 2A–2C, 4E, S1A, S3E, S3F, and S4B)
muIs84[(pAD76) sod-3p::GFP + rol-6(su1006)].	CGC	CF1553 (Figure 2D)
muIs84[(pAD76) sod-3p::GFP + rol-6(su1006)]; aptf-1(gk794) II.	This study	HBR2397 (Figure 2D)
kytEx1013[hsp-12.6p(5kb)::hsp-12.6:: GFP + rol-6(su1006)].	CGC, Honjoh et al.[35]	NIS1013 (Figure 2E)
kytEx1013[hsp-12.6p(5kb)::hsp-12.6:: GFP + rol-6(su1006)]; aptf-1(gk794) II.	This study	HBR2234 (Figure 2E)
eeEx106[hil-1::GFP + rol-6(su1006)].	CGC	EC106 (Figure 2F)
eeEx106[hil-1::GFP + rol-6(su1006)]; aptf-1(gk794) II.	This study	HBR2212 (Figure 2F)
zIs356[daf-16::GFP] IV.	Lin et al.[57] and this study	HBR2332 (Figures 4A–4D, and 6C)
zIs356[daf-16::GFP] IV; aptf-1(gk794) II.	This study	HBR2333 (Figures 4B, 4C, and 6C)
flp-11(syb1445) [flp-11-SL2-unc-58(L428F)-linker-mKate2] X.	Busack et al.[41]	HBR2340 (Figures 3B, 3C, 3E, 3G, and 4E)
flp-11(syb2193)[flp-11b-SL2(gpd-2)-mKate2-linker-twk-18(e1913)] X.	Busack et al.[41]	PHX2193 (Figures 3A, 3C, 3D, 3F, and 4E)
zIs356[daf-16::GFP] IV; flp-11(syb1445) [flp-11-SL2-unc-58(L428F)-linker-mKate2] X.	This study	HBR2482 (Figure 4C)
zIs356[daf-16::GFP] IV; flp-11(syb2193) [flp-11b-SL2(gpd-2)-mKate2-linker-twk-18(e1913)] X.	This study	HBR2572 (Figure 4C)
daf-16(mu86) I.	CGC	CF1038 (Figure 4E)
daf-16(mu86) I; aptf-1(gk794) II.	This study	HBR2546 (Figure 4E)
daf-16(mu86) I; flp-11(syb1445)[flp-11-SL2-unc-58(L428F)-linker-mKate2] X.	This study	HBR2545 (Figure 4E)
daf-16(mu86) I; flp-11(syb2193) [flp-11b-SL2(gpd-2)-mKate2-linker-twk-18(e1913)] X.	This study	HBR2547 (Figure 4E)
hsp-12.6::mKate2(syb1364) IV.	This study	PHX1364 (Figures 5A, 5C, 6D, 6E, S2A, S3A–S3D, and S4A)
hsp-12.6::mKate2(syb1364) IV; aptf-1(gk794) II.	This study	HBR2270 (Figures 5A, 5C, 6D, S2A, S3A–S3D, and S4A)
hsp-12.6::mKate2(syb1364) IV; *flp-11*(syb1445) *[flp-11-SL2-unc-58(L428F)-linker-mKate2] X.*	This study	HBR2379 (Figure 5A)
hsp-12.6::mKate2 (syb1364) IV; flp-11(syb2193) [flp-11b-SL2(gpd-2)-mKate2-linker-twk-18(e1913)] X.	This study	HBR2378 (Figures 5A and 6E)
hsp-12.6(gk156) IV.	CGC, C. elegans knockout consortium[58]	VC281 (Figure 5B)
hsp-12.6(gk196) IV; aptf-1(gk794) II.	This study	HBR2266 (Figure 5B)
hsp-12.6::mKate2 (syb1364) IV; daf-16 (mu86) I.	This study	HBR2319 (Figure 5C)

(*Continued on next page*)

Continued

REAGENT or RESOURCE	SOURCE	IDENTIFIER
hsp-12.6::mKate2(syb1364) IV; aptf-1 (gk794) II; daf-16 (mu86) I.	This study	HBR2320 (Figure 5C)
hsp-12.6::mKate2(syb1364) IV; daf-16 (mu86) I; flp-11(syb1445) [flp-11-SL2-unc-58(L428F)-linker-mKate2] X.	This study	HBR2666 (Figure 5C)
hsp-12.6::mKate2(syb1364) IV; daf-16 (mu86) I; flp-11(syb2193) [flp-11b-SL2 (gpd-2)-mKate2-linker-twk-18(e1913)] X.	This study	HBR2667 (Figure 5C)
goeIs304[pflp-11::SL1-GCaMP3.35-SL2::mKate2-unc-54-3'UTR, unc-119(+)] IV.	Wu et al.[29]	HBR1361 (Figures 6A and 6B)
goeIs304[pflp-11::SL1-GCaMP3.35-SL2::mKate2-unc-54-3'UTR, unc-119(+)] IV; mec-4(u253) X.	This study	HBR2782 (Figures 6A and 6B)
hsp-12.6::mKate2 (syb1364) IV; aak-1(tm1944) III; aak-2(ok524) X.	This study	HBR2464 (Figure S3A)
hsp-12.6::mKate2 (syb1364) IV; aak-1(tm1944) III; aak-2(ok524) X; aptf-1(gk794) II.	This study	HBR2465 (Figure S3A)
hsp-12.6::mKate2 (syb1364) IV; fkh-9(ok1709) X.	This study	HBR2461 (Figure S3B)
hsp-12.6::mKate2 (syb1364) IV; fkh-9(ok1709) X; aptf-1(gk794) II.	This study	HBR2462 (Figure S3B)
hsp-12.6::mKate2 (syb1364); daf-2 (e1370) III.	This study	HBR2345 (Figure S3C)
hsp-12.6::mKate2 (syb1364); aptf-1 (gk794) II; daf-2 (e1370) III.	This study	HBR2346 (Figure S3C)
hsp-12.6::mKate2(syb1364) IV; jnk-1(gk7) IV.	This study	HBR2477 (Figure S3D)
hsp-12.6::mKate2(syb1364) IV; aptf-1(gk794) II; jnk-1(gk7) IV.	This study	HBR2478 (Figure S3D)
daf-2(e1370) III.	CGC	CB1370 (Figure S3E)
daf-2(e1370) III; aptf-1(gk794) II.	This study	HBR1403 (Figure S3E)
hsp-12.6::mKate2(syb1364) IV; jkk-1(km2) X.	This study	HBR2454 (Figure S3F)
hsp-12.6::mKate2(syb1364) IV; aptf-1(gk794) II; jkk-1(km2) X.	This study	HBR2474 (Figure S3F)
hsp-12.6::mKate2(syb1364) IV; hsf-1(sy441) I.	This study	HBR2325 (Figures S4A and S4B)
hsp-12.6::mKate2(syb1364) IV; aptf-1(gk794) II; hsf-1(sy441) I.	This study	HBR2326 (Figures S4A and S4B)
hsp-12.6::mKate2(syb1364) IV; mec-4(u253) X.	This study	HBR2780 (Figures S5A and S5B)
hsp-12.6::mKate2 (syb1364) IV; aptf-1 (gk794) II; mec-4(u253) X	This study	HBR2781 (Figures S5A and S5B)
Bacterial strains		
Escherichia coli	CGC	OP50
Deposited data		
Raw and analyzed data	datadryad.org, data for all experiments, includes also the CeGaT transcriptome	https://doi.org/10.5061/dryad.cz8w9gj51
Original RNA-seq data	MPI-MG transcriptome, RNA-seq data for N2 vs HBR227, GEO	GSE196158
Original RNA-seq data	NCCT transcriptome, RNA-seq data for N2 vs HBR2340 and PHX2193, GEO	GSE196380

(Continued on next page)

Continued

REAGENT or RESOURCE	SOURCE	IDENTIFIER
Primers for genotyping		
Target gene	Forward	Reverse
aptf-1(gk794)	1. cgttcgtggatctcaatgtg 2. AGTTTTGGGGAATGGGGTAG	1. cggatcgattgctagagagg
RIS::unc-58gf(syb1445)	1. ACGAGGAAGACTTTGCTCCA	1. gacaccaatcaaattctagacagc 2. aaactcgcaaaaacgaggaa
RIS::twk-18(syb2193)	1. ACGAGGAAGACTTTGCTCCA	1. gacaccaatcaaattctagacagc 2. aaactcgcaaaaacgaggaa
daf-16(mu86)	1. cttcactcgccttcatcatc 2. GAACTCGATCCGTCACAATC	1. tgagtcgaaaaagctgagaaa
hsp-12.6::mKate2(syb1364)	1. CCCATAACTTCCTCCCAAAA	1. ttccggaaataatcgaattaaaaa 2. GATACGCATGGTTTGGGTTC
hsp-12.6(gk156)	1. tggagaaccgtctgtgtttt 2. CGAGGACCTGGAATCAAGTA	1. atgatgagcgttccagtgat
aak-1(tm1944)	1. AAGAAGATTTTCGGGCTTCT	1. TATGAAAACCAGGGCAGAAT 2. ATCGTGGAAGAATGAAAGGA
aak-2(ok524)	1. TCACTGGATGTCGTTGGAAA	1. GTTGGGAATACGCCAGCTAA 2. AGTAGTCAACGCCGGAAATG
fkh-9(ok1709)	1. acaacggtccagaagtgtcc	1. CGAAAAGCAAACAGGAGGTT 2. tcaaatattatggcaccacagc
daf-2(e1370)	1. TTCTGAATCGTCAAGGATCA 2. TCATTACTCAAACCAATATAGGG	1. TGACTATTATAAGCCATCGGG 2. TTACACTCGGTGCTCCGT
jnk-1(gk7)	1. cgcatcctcctcgatatcat 2. GTTGCGAAAAATCGGAACAT	1. cgaacgacaatgtttgatgg
jkk-1(km2)	1. aaatgtgtgcctggagaacg 2. CGCGATATAAAACCCTCGAA	1. cggcacatttttgttcacag
hsf-1(sy411)	1. ATAACAATTTTTCAGACATTTTTCGA 2. ACGGTACATTATTCCCAAAATCATACT	1. TCATCAAAATCTATATTCTCCAACTCTC 2. TTCAGAGATTTAGTCAGTAATCATAAGTG
mec-4(u253)	1. aggcaaaattgagccttctc 2. TTGCTCCATCAAATGCTGAC	1. attcccatgattggtgaagc
Software and algorithms		
NIS Elements Advanced Research 5.02	Nikon Instruments	https://www.microscope.healthcare.nikon.com/en_EU/products/software/nis-elements/nis-elements-advanced-research
MATLAB (version R2019a)	Mathworks	https://www.mathworks.com/products/matlab.html
g:Profiler	https://doi.org/10.1093/nar/gkz369	http://biit.cs.ut.ee/gprofiler/
Adobe Illustrator	Adobe	https://www.adobe.com/de/products/illustrator.html

RESOURCE AVAILABILITY

Lead contact

Requests for further information, resources and reagents should be directed to and will be fulfilled by the lead contact, Henrik Bringmann (henrik.bringmann@tu-dresden.de).

Materials availability

Key *C. elegans* lines that were used in this project are available at the Caenorhabditis elegans Genetics Center. Other *C. elegans* strains, or additional reagents generated for this study are available upon reasonable request from the lead contact.

Data and code availability

- The transcriptome data sets are deposited on dryad (CeGaT transcriptome) or at the GEO database (MPI-MG transcriptome and NCCT transcriptome) under the DOI or accession numbers listed in the key resources table.
- Raw and processed data for all experiments as well as MATLAB scripts used for analysis can be accessed at the DOI that is listed in the key resources table.
- All of the original data is available publicly as indicated above. Any additional information required to reanalyze the data reported in this paper is available from the lead contact upon request.

EXPERIMENTAL MODEL AND SUBJECT DETAILS

C. elegans strains were grown on Nematode Growth Medium (NGM) plates seeded with *Escherichia coli* OP50 and were kept at 20°C.[59] Deletion mutations and transgenic knock-ins were genotyped by Duplex PCR of single worms.[60] To confirm the presence of transgenes after crossings, fluorescent markers were used. The *C. elegans* strains used in this project are listed in the key resources table.

METHOD DETAILS

Generation of transgenic knock-in using CRISPR

The *hsp-12.6* allele that carries a c-terminal linker and mKate2 coding sequence was designed by us *in silico* to contain a linker sequence and an mKate2-coding sequence containing two artificial introns (underlined part of the sequence below, introns are displayed as small caps) inserted before the stop codon of *hsp-12.6*. The DNA was synthesized and the allele was generated by SunyBiotech as the strain PHX1364: *hsp-12.6(syb1364)* IV. Correctness was verified by using Sanger sequencing.

AGAAGCCCATAACTTCCTCCCAAAAGAGATTGAAGTCAAGAACATTGGAGAACTTCTTGAAATCCATATGGAGCACAATGTAAAG
AAGGATTCATTTGGAGATGTCTCTCGTAACATTACTCGTTGTTACAAACTTCCAAAGAATGTTGATATGAAGACAATCAAGAGCAAC
CTCGATTCACATGGAATTCTTCACATTGAAGCAAGAAAAATGCATGGATCCGGATCCGGA**ATG**TCCGAGCTCATCAAGGAGAACAT
GCACATGAAGCTCTACATGGAGGGAACCGTCAACAACCACCACTTCAAGTGCACCTCCGAGGGAGAGGGAAAGCCATACGAGG
GAACCCAAACCATGCGTATCAAGgtaagtttaaacatatatatactaactaaccctgattatttaaattttcagGCCGTCGAGGGAGGACCACTCCCATT
CGCCTTCGACATCCTCGCCACCTCCTTCATGTACGGATCCAAGACCTTCATCAACCACACCCAAGGAATCCCAGACTTCTTCAAG
CAATCCTTCCCAGAGGGATTCACCTGGGAGCGTGTCACCACCTACGAGGACGGAGGAGTCCTCACCGCCACCCAAGACACCTC
CCTCCAAGACGGATGCCTCATCTACAACGTCAAGATCCGTGGAGTCAACTTCCCATCCAACGGACCAGTCATGCAAAAGAAGAC
CCTCGGATGGGAGGCCTCCACCGAGACCCTCTACCCAGCCGACGGAGGACTCGAGGGACGTGCCGACATGGCCCTCAAGCTC
GTCGGAGGAGGACACCTCATCTGCAACCTCAAGgtaagtttaaacatgattttactaactaactaatctgatttaaattttcagACCACCTACCGTTCCAA
GAAGCCAGCCAAGAACCTCAAGATGCCAGGAGTCTACTACGTCGACCGTCGTCTCGAGCGTATCAAGGAGGCCGACAAGGAGA
CCTACGTCGAGCAACACGAGGTCGCCGTCGCCCGTTACTGCGACCTCCCATCCAAGCTCGGACACCGT**TAA**

Transcriptional profiling by RNA-sequencing

Sample preparation: Samples for bulk sequencing of N2, HBR227, HBR2340 and PHX2193 were generated by growing worms on Nystatin-supplemented plates (NEP), seeded with Na22 bacteria, at 20°C until they reach adulthood. The population was then synchronized by hypochlorite treatment.

For the CeGaT and MPI-MG transcriptomes, the following bleaching protocol was used:

1. Alkaline hypochlorite solution was prepared fresh and heated to 36°C. The solution loses its potency over time, even though it can be stored at 4°C up to a week. Hypochlorite solution is more effective when it is warm. However, heating hypochlorite solutions at high temperatures for prolonged periods of time produces toxic phosgene gas. Handle with care, since hypochlorite is a whitening agent and will bleach fabrics. The solution was made by mixing 6 ml NaOCl (15% w/v), 12.5 ml NaOH (1 M) and 31.5 ml sterile H_2O for a final volume of 50 ml.

2. Worms were grown on NGM plates until they became gravid adults. Then they were washed off with M9 buffer and transferred to an Eppendorf or Falcon tube, depending on the volume of buffer used.
3. Afterwards, the tube was put in ice for 2-3 min which allowed all the adult worms to sink to the bottom, while younger larval-stage worms were suspended in the supernatant. *C. elegans* larvae are particularly resistant to bleaching and their presence will cause over-exposure of the eggs to the bleach solution, killing them in the process. The supernatant was then discarded.
4. 500 μl of hypochlorite solution was added per 100 μl of adult worm pellet as well as an equal amount of M9. The tube was shaken vigorously for 1 min and then centrifuged at 4200 x g for 30 sec. This killed the worms without dissolving them and a compact pellet was formed. The supernatant was then discarded.
5. 1000 μl of hypochlorite solution was added per 100 μl of adult worm pellet. The tube was shaken vigorously for 1 min. Under the stereomicroscope it was observed that the cuticles had started to dissolve and the eggs were released. Then it was centrifuged at 4200 x g for 30 sec. The pellet should have a yellow color. The supernatant was then discarded.
6. 1000 μl of M9 was added per 100 μl of adult worm pellet, the pellet was resuspended and centrifuged at 4200 x g for 30 sec. The pellet should be white and nearly all of the adult cuticles should be dissolved. The supernatant was then discarded.
7. 2 more rounds of washing with M9 (Step 6 above) were performed. The pellet was suspended in an appropriate amount of M9 (usually 1 ml M9 in a 2 ml Eppendorf tube), which allowed enough oxygen for worm development. The final suspension should not have the characteristic hypochlorite smell.
8. The worms were let to hatch overnight while rotating (20 rpm) at 20°C. The next day, a healthy population L1 arrested worms should be swimming in the tube.

The hypochlorite treatment protocol for the samples HBR2340, PHX2193 and N2 (NCCT transcriptome) was slightly modified:

1. The hypochlorite solution was made by mixing 6ml NaOCl (15% w/v), 3ml NaOH (5 M) and 21ml sterile H_2O for a final volume of 30ml.
2. Worms were grown on NGM plates until they became gravid adults. Then they were washed off with M9 buffer and transferred to 2ml Eppendorf tubes.
3. Afterwards the worms were centrifuged at 9800rpm for 3min. The M9 supernatant was discarded.
4. 500 μl of hypochlorite solution was added. The tube was shaken vigorously for 30s and then centrifuged at 9800rpm for 30s. Upon centrifugation, the supernatant was removed.
5. 1000 μl of M9 was added, the pellet was resuspended and centrifuged at 9800rpm for 30 sec. The supernatant was discarded.
6. Steps 4 and 5 were repeated.
7. Afterwards, a third round of hypochlorite treatment was conducted by adding 500 μl of hypochlorite solution. However, this time the worms were not shaken and directly centrifuged for 30s at 9800rpm. Upon centrifugation, the supernatant was removed.
8. Finally, the worms were washed 3 times by executing step 5 twice and then resuspending the pellet in 1000 μl of M9 buffer.
9. Finally, the worms were kept in a rotator (20rpm) at 25°C for 48h until harvesting.

L1 arrested worms were harvested after 48 hours (“Starved”), at a final concentration of 20.000 worms/sample. The “Fed” samples were treated as described above, but were supplemented with OP50 for 4 hours after hatching. Then they were washed 3 times with M9 to remove the bacteria. The supernatant was aspirated from every sample and the pellet was flash frozen in liquid N_2 (CeGaT transcriptome, NCCT transcriptome) or suspended in 1 ml RNA-later ICE (Thermo Fisher Scientific) (MPI-MG transcriptome). Then samples were stored at -80°C overnight and shipped on dry ice for downstream processing.

Sequencing

The first transcriptome (CeGaT transcriptome) was carried out by a commercial supplier, CeGaT. CeGaT carried out the RNA extraction, library preparation and quality controls. Sequencing was carried out with an Illumina HiSeq 2500 platform at 30 M reads/sample, single-end (1x50bp). CeGaT mapped the sequencing data to the *C. elegans* genome and provided expression counts for all genes. A total of 3 replicates per condition were sequenced. Quality control with principal component analysis showed that samples: N2_A(starved), HBR227_A(starved), N2_B(fed) and HBR227_C(fed) did not cluster with the others and were removed from the downstream analysis. See Data S1.

The second transcriptome (MPI-MG transcriptome) was generated at the Max Planck Institute for Molecular Genetics by S.B. and B.T. The samples were sequenced with an Illumina HiSeq 4000 platform at 50 M reads/sample, paired-end (2x50bp). FASTQ files were received and they were annotated to the *C. elegans* genome by Jik Nijssen, providing expression counts for all genes. A total of 4 replicates per condition were sequenced. Quality control with principal component analysis showed that the sample HBR227_A did not cluster with the others and was removed from the downstream analysis. See Data S3.

The third transcriptome (NCCT transcriptome, the transcriptome for HBR2340, PHX2193 and N2) was carried out by the NCCT NGS Competence Center of Tübingen. RNA was extracted via the QIAsymphony RNA Kit. Library preparation and quality controls were carried out by the sequencing center. Sequencing was carried out with an Illumina NovaSeq6000 (25 M paired-end reads 2x100bp). The data was mapped by the NCCT to the *C. elegans* genome resulting in expression counts per gene. FASTQ files and gene-expression count tables were received. A total of 4 replicates per condition were sequenced. Quality control with principal

component analysis showed that the sample N2_C did not cluster with the others and was removed from the downstream analysis. See Data S5.

Proteomic characterization of *C. elegans*

Sample processing: *C. elegans* cultures of strains N2 and HBR227 were grown by A.K. as described above for transcriptome analysis. Per sample, $5x10^4$ worms were collected by centrifugation and flash-frozen in liquid N_2. Then, samples were shipped on dry ice for downstream processing.

TMT labeling and quantitative MS was carried out by L. M. W., A. W., and H. U.. Worms were ground in liquid N_2 and lysed by addition of 100 mM HEPES/HCl pH 7.5, 4% SDS, 1 mM EDTA. Mechanical breakdown was performed by addition of 1 volume 0.7 nm Zirconia Beads (BioSpec) and three cycles of beating for 20 s at 5.5 m/s with 15 s breaks using a FastPrep-24™ Bead Beating Grinder (MP Biomedicals). TEAB pH 8 was added to a final pH of 8. Proteins were reduced, alkylated and acetone-precipitated. Pellets were dissolved in 50 mM TEAB and trypsin was added in a 1:20 enzyme-to-protein ratio following ON digestion. TMT-6plex labeling was performed according to manufacturer's instructions. After labeling, peptides were desalted using pre-packed C18 spin columns (Harvard Apparatus) and concentrated in a SpeedVac. Labeled peptides were pre-fractionated using Agilent 1100 series HPLC system equipped with a C18-X-Bridge column (3.5 μm particles, 1.0 mm inner diameter, 150 mm length; Waters). The HPLC was operated at a flow rate of 60 μl/min using a buffer system of: Buffer A: 10 mM NH_4OH and Buffer B: 10 mM NH_4OH and 80% (v/v) ACN. Peptide separation was performed over 94 min using a linear gradient from 10% to 55% buffer B in 68 min. One-minute fractions were collected and pooled into 25 fractions in total. Peptide samples were dried in a SpeedVac.

LC-MS/MS measurements: Labeled and fractionated peptides were dissolved in 2% [v/v] acetonitrile, 0.05% [v/v] TFA. LC-MS/MS analyses were performed on an Orbitrap Fusion™ Lumos™ Tribrid™ Mass Spectrometer (Thermo Fisher Scientific) coupled to a nanoflow liquid chromatography system (Thermo Scientific Dionex Ultimate 3000). Sample separation was performed over 90 min at a flow rate of 300 nl/min using 0.1% [v/v] formic acid (buffer A) and 80% [v/v] acetonitrile, 0.08% [v/v] formic acid (buffer B) and a linear gradient from 7% to 45% buffer B in 64 min. Peptides were analyzed in positive mode using a data-dependent top speed acquisition method with a cycle time of 3 s. Resolution was set to 120,000 (MS1) and 15,000 FWHM (MS2). AGC targets were set to $4x10^5$ (MS1) and 10^5 (MS2), normalized collision energy to 35%, dynamic exclusion to 15 s, and maximum injection time to 40 (MS1) and 30 ms (MS2). See Data S2.

Label-Free Quantification: Samples were prepared as above by A.K. and the proteome analysis by Label-Free Quantification (LFQ) was carried out by D.M. as described previously.[61] See Data S4.

Survival and lifespan of L1 arrested animals

We carried out survival and lifespan measurements. For survival experiments, the fraction of surviving animals in a suspension of worms was measured by drawing a sample at regular time intervals. For lifespan experiments the larvae were observed during defined time points until they died. For these lifespan experiments, larvae were kept inside microfluidic devices.

Survival measurements of L1 arrested animals was carried out as described.[29] Briefly, worms were synchronized by hypochlorite treatment and transferred to 2 ml Eppendorf tubes, at a concentration of 10.000 worms in 1 ml of M9 buffer. The tubes were strapped on a rotating device (20 rpm) and placed inside a 20°C incubator. Measurement of survival was carried out once per day. For measurements of the survival, 10 μl of the worm suspension was pipetted onto NGM plates seeded with OP50 and the total number of worms was counted. One day later, worms were scored as "dead" if they did not show any signs of movement (e.g. traces on the bacterial lawn) and were immobile.

For the lifespan chamber assays, 3-fold stage eggs were picked in 110 x 110 x 10 μm chambers without food. A heating lid (20 °C) was fit on the top of the petri dish to keep the temperature constant and prevent drying of the agarose. The animals were scored for survival every day by evaluating their response to blue light (1.75 mW/mm^2, 490 nm). When an animal failed to respond to 2 minutes of blue light stimulation, it was scored as dead. Detailed results can be found in Data S7.

Long-term imaging using agarose hydrogel micro-chambers

Long-term imaging of L1 arrested worms was performed in agarose hydrogel microchambers as described previously.[44,45] Briefly, a poly-dimethyl-siloxane (PDMS) mold, activated by air plasma exposure for 30 s, was used to cast micro-compartments from 1 ml of 5% high gelling temperature agarose (Sigma-Aldrich) dissolved in M9 buffer and heated to about 95°C. The chamber size was 110 x 110 x 10 μm. By using a platinum worm pick, the chambers were filled with 3-fold-stage eggs without food, sealed with a glass coverslip and glued with double-sided adhesive tape into a square (2 x 2 cm) opening, milled in a 35 x 10 mm plate. The plate was filled with 2 ml of agarose, which would act as a moisture reservoir, and sealed with Parafilm M (Sigma-Aldrich) to prevent moisture loss. Chambers were incubated with the plastic dish placed upside down into an incubator at 20°C until use.

Fluorescence imaging in L1 arrest

Fluorescence-tagged transgene expression was quantified by fluorescence microscopy. An "Eclipse Ti" microscope (Nikon) with an automated XY stage (Nikon), a digital DS-Qi2 camera (SLR, FX-format CMOS sensor, Nikon) and a 40x/0.75 Plan Fluor Oil objective lens (Nikon) were used combined with an additional built-in 1.5x lens for a total magnification of 60x. A custom-made heating lid was used to keep the temperature constant at 25.5°C to avoid condensation (sample temperature was measured at 23.5°C). The software used for image acquisition and microscope control was "NIS elements" (Nikon). For GFP and mKate2 excitation, an LED system

(CoolLED) provided light at 490 nm and 565 nm, respectively. Exposure time was set to 100 ms and EM Gain to 1.0x. Light intensity was measured to be 1.75 mW/mm^2 for 490 nm and 0.517 mW/mm^2 for 565 nm illumination, using an optical power meter (PM100A, Thorlabs). A standard set of GFP and Texas Red filters were used for light filtering. Camera resolution was 14-bit 808 x 808.

Reporter transgene expression was measured either continuously for 3 days (1 frame every 15 or 30 min) or once every 24 hours for up to 12 days. Average fluorescence intensity was quantified per worm after background subtraction, assuming that the size of the worm is 10% of the total image size. For the continuous 3-day imaging experiments, frames were extracted from the movies and aligned to the point of hatching. Frames that were collected before hatching were excluded from downstream analysis. At least 8 animals were imaged per strain in at least 2 chambers (biological replicates). For the daily measurement experiments, chambers were made in the evening of the day prior to the start of the experiment (Day 0). That gave the eggs a time interval of 10-12 hours to complete embryogenesis and hatch but not yet starve. At least 20 animals were imaged per strain in 1 to 3 chambers (biological replicates). The chambers were kept in a 20°C incubator when not being imaged.

Heat shock

For the heat shock experiment, worms were imaged right after hatching. Then the microchamber was placed in the 32°C incubator for 24 hours and the worms were imaged again.

GCaMP imaging

GCaMP 3.35 was expressed in RIS using the *flp-11* promoter. 3-fold-stage eggs were placed in agarose microchambers (110 x 110 x 10 μm) and imaged with a Nikon Eclipse Ti microscope, using an iXon Ultra EMCCD (1,024 × 1,024 pixels) (Andor Technology Ltd.). The camera and a 40x/0.75 Plan Fluor Oil objective lens (Nikon) were used combined with an additional built-in 1.5x lens for a total magnification of 60x. For GFP excitation, an LED system (CoolLED) provided light at 490 nm. Exposure time was set to 100 ms and EM Gain to 1.0x. Light intensity was measured to be 1.6 mW/mm^2. A standard set of GFP and Texas Red filters were used for light filtering.

Mechanical stimulation

Mechanical stimulation of the worms was carried out as described previously[51,62] in 110 x 110 x 10 μm microchambers without food, made of 5% high gelling temperature agarose (Sigma-Aldrich) dissolved in M9 buffer. A piston (2.5 mm in diameter) was driven into the chamber at the xy-plane, by the use of an electromagnet and the whole setup was fitted in a custom-made aluminum holder. To avoid habituation, a set of 5 taps were delivered every 5 minutes and the time interval between taps was 1 second. This protocol has been shown previously to efficiently disturb sleep and to trigger DAF-16::GFP nuclear localization.[49] The signal for triggering the tapping stimulus was generated by the use of an Arbitrary Waveform Generator (Hewlett Packard, 33120A), which created square waves with amplitude 5 V and frequency 5.000 mHz. This signal was further amplified at 24 V, by a TTL signal amplifier. A heating lid, set to 22°C, was fit on the chamber to keep it from drying out (sample temperature: 20°C). The tapping stimulus protocol was started around 8–10h after mounting the eggs in the microfluidic devices, a time at which the egged had hatched. The tapping stimulus protocol was applied continuously until the end of the experiment, i.e. until all animals had died. For imaging DAF-16::GFP localization, the plastic dish containing the agarose microchambers was taken off the tapping device and transferred to a widefield microscope for fluorescent imaging. The dish was then placed back to the tapping device. The imaging took around 10 minutes, during which the tapping protocol was interrupted. The chambers were imaged once per day to assess transgene expression or DAF-16 localization. To quantify RIS GCaMP intensity the chambers were imaged continuously (1 frame every 2 seconds, applying the mechanical stimulation protocol consisting of 5 taps, constituting one trail, each trial was repeated three times with a time delay between tapping of 1h.

Quantification of DAF-16::GFP nuclear localization

Strains that expressed the *zIs356[daf-16::gfp]* transgene were imaged in 110 x 110 x 10 μm microchambers without food, made of 5% high gelling temperature agarose (Sigma-Aldrich) dissolved in M9 buffer. A heating lid, set to 22°C, was fit on the chamber to keep it from drying out (sample temperature: 20°C). Images were taken either daily or continuously (1 frame every 30 seconds) on an "Eclipse Ti" microscope (Nikon) with an automated XY stage (Nikon), a digital DS-Qi2 camera (SLR, FX-format CMOS sensor, Nikon) and a 40x/0.75 Plan Fluor Oil objective lens (Nikon) were used combined with an additional built-in 1.5x lens for a total magnification of 60x. Exposure time was set to 100-400 ms and EM Gain to 1.0x. Most of the data was acquired with 100 ms exposure time. One data set in the wild-type background was acquired with an exposure time of 400 ms. The longer exposure time caused a blurring of some of the frames. Yet, this did not appear to change the conclusions and hence this replicate was kept in the analysis. Light intensity was measured to be 1.75 mW/mm^2 for 490 nm and 0.517 mW/mm^2 for 565 nm illumination, using an optical power meter (PM100A, Thorlabs). A standard set of GFP and Texas Red filters were used for light filtering. Camera resolution was 14-bit 808 x 808. See Data S6.

QUANTIFICATION AND STATISTICAL ANALYSIS

Transcriptional profiling by RNA-sequencing and GSE analysis

Differential expression analysis and downstream analysis was carried out by A.K. through a custom-written MATLAB script. All transcriptomes were analyzed in the same way. p-values were corrected for false discovery rate by the Benjamini-Hochberg method.

Significance thresholds were set as follows: $|\log_2 FC| > 1$ and FDR < 0.05. This was implemented in order to account for biological significance. However, genes with smaller fold changes were also considered for downstream Gene Set Enrichment analysis, performed with the online tool "g:Profiler", using the default settings.[63] For tissue-specific and *daf-16*-related GSE, published datasets were used.[32,64,65] Statistical significance was assessed with Fisher's exact test and p-values were adjusted using the Bonferroni correction. See Data S1, Data S3, and Data S5.

Proteomic characterization of *C. elegans*

TMT6 data were analyzed with MaxQuant version 1.5.5.1[66] using default settings and quantification based on MS2 reporter ions (TMT6plex). Canonical protein sequences from *C. elegans* were downloaded from Uniprot (reviewed, 03.04.2013). Further analyses were performed using Perseus version 1.5.6.0.[67] A.K. filtered the protein groups for a minimum of one unique peptide, $\log_2$ transformed the intensity values and calculated the fold changes. See Data S2.

Label-Free Quantification samples were analyzed by D.M. as described previously.[61] See Data S4.

Survival and lifespan of L1 arrested animals

Survival measurements of L1 arrested animals estimated by using the Kaplan-Meier method, significance assessment was done by using Fisher's exact test for every time point, p-values were corrected for false discovery rate by the Bonferroni method and the significance threshold was set to $p_{adj} < 0.05$. Finally, the point of 50% survival was determined by fitting a 6th degree polynomial to the survival curve. For the lifespan chamber assays, survival was estimated by using the Kaplan-Meier method and significance was assessed with the log-rank test. Detailed results can be found in Data S7.

Fluorescence imaging in L1 arrest

Worms that died before or during the measurement period were omitted from downstream analysis. Single worms with transgene intensities > Q3 + 1.5 * IQR or transgene intensities < Q1 + 1.5 * IQR for every time point of the analysis, were scored as outliers and omitted from further analysis (Q1 = 25th percentile, Q3 = 75th percentile, IQR = Interquartile range). Significance was assessed at every time point by the 2-tailed Welch's t-test (assuming unequal variances), the resulting p-values were corrected for false discovery rate by the Benjamini-Hochberg method and FDR < 0.05 was selected as the significance threshold. In every case, error bars denote the standard error of the mean.

GCaMP imaging

The position of the RIS neuron was detected and the intensity was quantified with a custom-made MATLAB script based on an empirically defined intensity threshold.

RIS intensity was normalized as follows:

$$[(\text{RIS intensity at every time point}) - (\text{Min RIS intensity})]/[(\text{Max RIS intensity}) - (\text{Min RIS intensity})]$$

We used the 0.5th and 99.5th quartile to determine the Minimal and Maximal RIS intensity:

Min RIS intensity = average of the lowest 0.5% of values

Max RIS intensity = average of the highest 0.5% of values

Normalization was carried out for every individual worm, so that the intensities were within the range of 0 – 1.

The position of the RIS neuron was used to determine motion speed. For detecting quiescence, a threshold cutoff of < 0.20 of the maximum speed for each individual was used. In a previous study[39] we imaged quiescence over several days and applied a threshold to extract quiescence bouts only that were longer than 2 minutes. As for this experiment we were looking at behavioral changes that occur upon tapping, which lasts just a few seconds, and the corresponding movies are much shorter, we did not apply any bout length threshold. This leads to an increase in detectable behavioral quiescence in Figure 6B of this paper compared to Figure 3A in our previous paper.[39]

Mechanical stimulation

The strongest increase in calcium signals upon stimulation is typically observed in the first 5 s after the stimulus, see for example Suzuki et al.[53] We hence used a time window of 10 s, which thus includes the majority of the calcium transient. We matched the analysis of behavior to the window for analysis of calcium changes. For the time window following the peak we also used a time window of 10 s for consistency.

Quantification of DAF-16::GFP nuclear localization

The DAF-16::GFP images were further processed by a custom-written MATLAB script. Briefly, the script detected circular areas with radii in the range of 2-8 pixels and the total GFP intensity in these areas was summed up. Wild-type movies were assessed frame-by-frame and compared to their respective GFP intensity values. From this comparison the following thresholds were acquired for: GFP < 5000 units "Cytoplasmic", 5000 < GFP < 10000 units "Intermediate" and GFP > 10000 units "Nuclear". These thresholds were selected empirically to describe the localization of DAF-16 at any time point. All images could be assessed with this method an no animals were censored.

Statistical significance was assessed with two-way ANOVA with correction for multiple comparisons with Tukey's honest significant difference criterion. A two-way ANOVA was performed to compare the effect of 1) RIS activation state and 2) time spent in L1 arrest, on DAF-16 localization. We found a statistically significant difference in DAF-16 localization affected by both RIS activation state (d.f. = 3, F = 49.3, p-value = 4.38×10^{-11}) and time spent in L1 arrest (d.f. = 4, F = 13.46, p-value = 3.72×10^{-06}), as well as the interaction between these two terms (d.f. = 12, F = 3.32, p-value = 0.0047). Post-hoc correction for multiple comparisons with Tukey's honest significant difference criterion, revealed significant pairwise difference in DAF-16 localization between the ''Wild type (Control)'' and ''Wild type (Tap)'' conditions (Difference = 24.8 ± 6.71 %, $p_{adj} = 4.429 \times 10^{-09}$), while there was no significant difference between the ''*aptf-1(gk794)* (Control)'' and ''*aptf-1(gk794)* (Tap)'' conditions (Difference = 1.94 ± 7.06 %, $p_{adj} = 0.8751$). Detailed results can be found in Data S6.